CHAPTER 6: BEXAROTENE

6.1. Introduction:

Chemically, Bexarotene (BXR) is a synthetic retinoid and these retinoids are vitamin A analogues. It binds to nuclear retinoid receptors *i.e.* retinoic acid receptor (RAR) and/or retinoid X receptor (RXR). This ligand-bound receptor forms dimeric complexes which interact with DNA at specific retinoid-responsive elements and regulate the transcription of target genes and thereby it controls the cellular proliferation, differentiation, and apoptosis. BXR is a selective agonist of retinoid X receptor (RXR) and it binds to all three isomers of this receptor *i.e.* RXRα, RXRβ and RXRγ with identical affinity and potency. BXR inhibits the cell growth and induces the differentiation and thereby it promotes the apoptosis in the tumor cells and thus exhibits the anti-cancer activity. It has already been approved by the food and drug administration (FDA) to treat skin issues caused by cutaneous T-cell lymphoma that is unresponsive to different medicines (1). Additionally, BXR also has remarkable anti-tumor activity against lung cancer, breast cancer and prostate cancer (2, 3). Furthermore, it is effective in preventing ER-negative mammary tumorigenesis in mice, and had less toxicity than other retinoids (4). Thus, retinoids represent more effective and more tolerable class of agents for the prevention of breast cancer.

Though having potential applications as anti-tumor moiety, it also faces the solubility issues similar to most of the NCEs. It belongs to the BCS class II category and thus its clinical activity is limited by its solubility. Formulating a nano level delivery system may significantly improve its solubility characteristic and this in turn will be helpful in the improvement of bioavailability of the same.

In the present work we have studied the influence of 2D and 3D pore structure along with effect of surface functionalization on the dissolution and bioavailability profile of BXR. Surface decoration using amine moiety gave a controlled release of the cargo from the pores. Furthermore, stimuli responsive smart polymeric drug delivery system is gaining an attention now a days especially in tumor targeting. Among others pH responsive ligands, hyaluronic acid constitutes appealing properties with respect to biocompatibility, biodegradability and non-immunogenic toxicity, making it ligand of choice as both capping and targeting agents (5). HA is used as a targeting agent due to its selective affinity towards CD44 receptors which are overexpressed in many types of tumor cells. Therefore, HA serves as an excellent tumor targeting agent (6).

In the present chapter, how MSNs improve the *in vitro* release profile and *in vivo* pharmacokinetics behaviour of BXR is discussed in details. Further, the application of HA functionalized MSNs as a dual responsive drug delivery system (the pH triggered and receptor-based drug release) has also been deliberated in depth.

6.2. Materials and methods:

6.2.1. Chemicals and reagents

An active pharmaceutical ingredient Bexarotene (BXR ≥99%) was obtained as a sample gratis from Apicore Pharmaceutical Ltd, Vadodara, Gujarat, India. Other ingredients like fumed silica, tetra methyl ammonium hydroxide pentahydrate (TMAOH; ≥98%), tetraethyl orthosilicate (TEOS; ≥99%), cetyl trimethyl ammonium bromide (CTAB; ≥99%), (3-aminopropyl) triethoxysilane (APTES; ≥99%) utilized in the synthesis of MSNs were procured from Sigma Aldrich (USA). Deionized water was used in the synthesis of MSNs.

HPLC grade methanol (MeOH) and acetonitrile (ACN) were procured from Fisher Scientific (Vadodara, Gujarat) to carry out chromatographic analysis. Different reagents utilized during dissolution and diffusion study like hydrochloric acid (HCl), potassium dihydrogen phosphate, acetic acid, ammonium formate, formic acid, polysorbate-80, hydrochloric acid, sodium acetate trihydrate, acetic acid, monobasic potassium phosphate and sodium chloride were acquired from Loba Chemie (Mumbai, Maharashtra). Unless otherwise stated, all chemicals were utilized as received and reagents were of analytical grade.

The cytotoxicity study was carried out on an *in vitro* model of epithelial cells *i.e.* Caco-2 (for oral formulation) and MCF-7 (for parenteral formulation) which were procured from the National Centre for Cell Science (NCCS, Pune, India) and the cells were cultured in T-25 cm^2 tissue culture flask supplemented with Dulbecco's modified eagle medium (DMEM) media supplemented with 0.1% penicillin and streptomycin solution and 20% and 10% foetal bovine serum (FBS). The culture medium was replaced after every alternative day. Cell culture grade dimethyl sulphoxide (DMSO ≥99%) and other culture solutions mentioned before were procured from Himedia laboratories. The 3-(4, 5-Dimethylthiazol-2-yl)-2, 5-diphenyltetrazolium bromide (MTT) dye was purchased from Sigma Aldrich (USA). Fluorescein isothiocyanate (FITC) and 4,6-Diamidino-2-Phenylindole Dihydrochloride (DAPI) were purchased from SRL chemicals (Mumbai). Various well plates and other materials used in the cell line study were purchased from HI media Laboratories.

Female Swiss albino mice (body weight, 20 ± 2 g) were supplied by ZydusCadila healthcare Ltd, Gujarat, India. All the animal experiments performed in accordance with the protocols approved by the Institutional animal ethics committee (IEAC) guidelines having protocol number MSU/IAEC/2017-18/1725. The mice were acclimatized to the laboratory environment for a week with free water and food access before conducting the actual experiment.

6.2.2. Synthesis of MSN-41 and MSN-48 types of Nanocarriers:

The mesoporous silica carriers (MCM-41 and MCM-48) used for RLX loading were unable to accommodate BXR in the because of its small pore size, therefore the large pore MSNs *i.e.* large pore MCM-41 and MCM-48 were synthesized.

6.2.2.1. Synthesis of large pore MCM-41

MCM-41 synthesis was carried out by a template based synthesis approach as per the method reported in literature (7) Briefly, the synthesis of NPs was accomplished by the preparation of a reaction mixture having composition of 1 H_2O: 0.06 SiO_2: 0.02 TMAOH: 0.01 CTAB: 0.01 NH_4OH. The resultant slurry was given hydrothermal treatment at 343 K for 3 days succeeded by sample ageing step in the mother liquor at 423 K in Teflon lined autoclave for 2 days. Later on, the as-synthesized product was recovered by filtration and further washed and dried. Eventually, template free MCM-41 NPs were obtained by calcination of dried product at 823 K.

6.2.2.2. Synthesis of large pore MCM-48

The MCM-48 synthesis was carried out as per the literature reported method. Concisely, the reaction mixture having composition of 1TEOS: 12.5 NH_3: 54 EtOH: 0.4 template: 174 H_2O was prepared. This was done by sequential addition of all aforementioned ingredients followed by continuous agitation for 2 h to obtain a homogeneous reaction mixture. The prepared homogeneous reaction mixture was filtered, washed and dried at the ambient temperature. The template removal was achieved by calcination at 823 K for 6 h (8).

6.2.2.3. Synthesis of amine coated MCM-41 and MCM-48 nanoparticles:

The identical surface functionalization methodology was adopted for both MCM-41 as well as MCM-48. External grafting of amine moiety was secured following post synthetic grafting approach with few modifications (9, 10). Wherein, the dispersion of 0.1 grams MSNs in 25 mL toluene was treated with the 1.38 mL of APTES followed by refluxing the reaction mixture at 120 ºC for 24h. Subsequently, the obtained slurry was filtered and acquired material was labelled as MCM-NH_2-41 and MCM-NH_2-48.

6.2.2.4. Synthesis of large pore hyaluronic acid coated MCM-41 and MCM-48 nanoparticles:

Accurately weighed 1g of amine coated nanoparticles (MCM-NH_2-41 and MCM-NH_2-48) were dispersed in 100 mL deionized water. On the other side, 20mL of an aqueous solution of

EDC: NHS (0.2:0.37g) was mixed with HA aqueous solution (113mg/60 mL). Ultimately, both the reaction mixture was mixed together and the pH was adjusted to 9.0 using TEA. The mixture was stirred overnight, centrifuged and washed thoroughly and finally freeze dried to obtain MCM-HA-41 and MCM-HA-48 (11).

6.2.3. Drug loading inside the nanopores:

A novel immersion-solvent evaporation method was employed for encapsulation of BXR inside the mesopores (12). Briefly highly concentrated methanolic BXR solution (5000 µg/mL) was prepared and MCM-41, MCM-NH_2-41, MCM-HA-41 and MCM-48, MCM-NH_2-48, MCM-HA-48 were dispersed individually to have 1:1.5 drug: carrier mass ratio. This dispersion was stirred vigorously and subsequently subjected to rotary evaporation to obtain a dried BXR incorporated nanoparticles. The secured drug filled nanoparticles were termed as BXR-41, BXR-NH_2-41, BXR-HA-41 and BXR-48, BXR-NH_2-48, BXR-HA-48 respectively. %Drug loading and %entrapment efficiency was determined by UV-VIS spectrometry at 262 nm wavelength for BXR using below equations.

$$\%Entrapment\ Efficiency = \frac{Total\ weight\ of\ BXR\ present\ in\ nanoparticles}{Weight\ of\ BXR\ added\ initially} \times 100 \ldots\ldots\ldots\ldots\ldots 6.1$$

$$\%Loading\ Efficiency = \frac{Total\ weight\ of\ BXR\ present\ in\ nanoparticles}{Total\ weight\ of\ drug\ loaded\ nanoparticles} \times 100 \ldots\ldots\ldots\ldots\ldots 6.2$$

Further confirmation of %loading efficiency was done by TGA analysis. BXR loaded nanoparticles and BXR pure drug were subjected to thermal analysis up to 700 ºC with the heating rate of 5 ºC/min. %Loading results were divulged by plotting graphs of %weight loss versus temperature (ºC).

6.2.4. Solid state evaluation of pristine and functionalized MSNs.

The characterization of formulated BXR free and BXR filled nanoparticles nanoparticles were proceeded in the sequential manner. The synthesized MSNs were characterized for confirmation of the mesoporous skeleton integrity, for success of drug uptake, surface properties *etc* employing various characterization techniques. The methodology followed for characterization was kept identical as discussed in the previous section 5.2.4.

6.2.5. Elemental detection and Quantification of surface moiety:

6.2.5.1. Elemental detection:

An elemental detection for pristine and surface decorated nanoparticles was performed in order to investigate the presence surface elements for bare and surface functionalized nanoparticles adopting SEM-EDX (scanning electron microscopy-energy-dispersive X-ray spectroscopy) analysis conducted on FEI-quanta 200 model (Thermo Scientific, USA).

Further, the presence of carbon and nitrogen moiety after amine and hyaluronic acid grafting was done by SEM-EDX analysis of respective nanoparticles.

6.2.5.2. Quantification of surface grafted moieties:

6.2.5.2.1. Quantification of amine group:

An estimation of the amine group grafted over the external surface was carried out by performing Ninhydrin colorimetric assay (13, 14) and thermal method (15, 16). An identical approach was followed as mentioned in the previous section 5.2.5.2.1.

6.2.5.2.2. Quantification of other groups:

The thermal method was adopted for quantification of hyaluronic acid moiety present on the outer surface. Wherein, surface modified nanoparticles were given thermal treatment up to 700 ºC keeping heating rate of 5 ºC/min^{-1} and the %weight loss for both was calculated and ultimately the %attachment was calculated by following equations.

$$\%W_{HA} = \%W_{MSN-HA-41} - \%W_{MSN-41} \ldots\ldots\ldots\ldots\ldots 6.3$$

6.2.6. Formulation of laboratory mixture of BXR and evaluation:

As the commercial formulation of BXR is in capsule form. The physical mixture of BXR was prepared as it was not available in the local market. The mixture was prepared by combining various excipient altogether within their range along with BXR equivalent to 75mg in mesoporous carrier. The assay was performed by taking six replicates and %assay was reported (table 6.1).

Table 6.1. List of excipients used in preparation of physical mixture

Sr. No.	Name of Excipients	Application	Amount
1	Talc	Glidant + Diluent	0.5-1%
2	PEG	Lubricant	2-5%
3	Magnesium Stearate	Lubricant + Diluent	0.5-1%
4	Microcrystalline cellulose	Diluent	Q.S.

6.2.7. In vitro release study:

6.2.7.1. *In vitro* dissolution study:

Drug dissolution or drug release is a critical step as it has a significant influence on the bioavailability of the interested drug candidates suffering from solubility issues especially those belong to a BCS class II and IV category (17). *In vitro* dissolution study was performed for oral formulations of BXR in different dissolution media as listed in table 6.2. The *in vitro* release study was carried using Veego USP type II dissolution apparatus wherein the plain API, physical mixture, BXR-41, BXR-48, BXR-NH_2-41, BXR-NH_2-48 were subjected for rotation at a speed of 50 rpm in 900 mL dissolution media maintained at 37 ± 0.5 ℃ temperature. The study was also conducted in biorelevant media. The composition for all dissolution media is listed in the following table 6.2.

Table 6.2: Composition of different simulated and biorelevant dissolution media (18, 19)

Sr. No.	Ingredients	A	B	C	D	E	F	G
1.	Conc. HCl	7 mL	-	-	q.s. to get pH 1.6	q.s. to get pH 1.6	-	-
2.	Sodium acetate trihydrate	-	2.99 gm	-	-	29.75 mM	-	-
3.	acetic acid	-	14.0 mL (2 N acetic acid)	-	-	17.12 mM	-	8.65 gm
4.	Sodium hydroxide	-	-	0.616 gm	-	-	34.8 mM	4.04 gm

5.	Monobasic potassium phosphate	-	-	6.8 gm	-	-	-	-
6.	Sodium chloride	2 gm	-	-	1.9986 gm (34.2 mM)	237.02 mM	68.62 mM	11.874 gm
7.	Pepsin	3.2 gm	-	-	0.1 gm (0.1 mg/mL)	-	-	-
8.	Pancreatin	-	-	1 gm		-	-	-
9.	Sodium taurocholate	-	-	-	0.4125 gm (0.08 mM)	-	3 mM	15 mM
10.	Lecithin	-	-	-	0.1287 gm (0.02 mM)	-	0.2 mM	3.75 mM
11.	milk	-	-	-	-	500 mL	-	-
12.	Maleic acid	-	-	-	-	-	19.12 mM	-
13.	Polysorbate 80	0.1%	0.1%	0.1%	-	-	-	-
14.	Deionised water	Upto 1000 mL	Upto 1000 mL	Upto 1000 mL	Upto 1000 mL	Upto 1000 mL	Upto 1000 mL	Upto 1000 mL

A: Simulated gastric fluid (SGF pH: 1.8), B: Sodium acetate buffer (pH: 4.5), C: Simulated intestinal fluid (SIF) (pH: 6.8), D: Fasted state simulated gastric fluid (FaSSGF) (pH: 5), E: Fed state simulated gastric fluid (FeSSGF), F: Fasted state simulated intestinal fluid (FaSSIF-V2), G: Fed state simulated intestinal fluid (FeSSIF)

6.2.7.2. *In vitro* diffusion study:

The drug release study from the parenteral formulation was evaluated following *in vitro* diffusion study performed in dialysis bag. The release study was performed at three different pH of the phosphate buffer saline (PBS) solution *i.e.* at pH 5.6, 6.8 and 7.4. Herein, 10 mg of the formulation was dispersed in 5 mL dispersion media and filled in the dialysis bag. The bag was immersed in 100 mL diffusion media and rotated at 75 rpm. The temperature of the assembly was maintained at 37 ºC and the aliquots were withdrawn at different time interval up to 72 h. The samples were analyzed by RP-HPLC method and %CDR was calculated.

6.2.8. In vitro cytotoxicity Study:

Two different cell lines were used to perform *in vitro* cytotoxicity study *viz.*, Caco-2 cell line (for oral formulation) and MCF-7 cell line (for parenteral formulation).

6.2.8.1. Caco-2 cell line:

Herein, MTT assay was performed on Caco-2 cells before initiating the cell permeability study in order to select the maximum safe concentration of BXR encapsulated pristine and amine coated nanoparticles which will not harm the cell viability. The formulation having BXR concentration ranging from 10 ppm to 100 ppm were taken to proceed further with the MTT assay. Here in the experiment started with the seeding step, where the Caco-2 cells were cultured in 96 well plates using DMEM medium enriched with sodium pyruvate, L-glutamate, sodium bicarbonate along with high glucose and supplemented with 20% fetal bovine serum (FBS) and 1% penicillin-streptomycin (Pen/strep) solution which resist bacterial growth. Once the cell growth reached to $1*10^4$ cell/well density, the cell was given nanoparticle treatment. Eventually, the cells were treated with MTT dye after a desired period of time and evaluated for cell viability parameter at 570 nm using plate reader. Furthermore, the blank and negative control readings were also taken in order to avoid false negative errors. The cells without nanoparticle treatment was taken as a negative control and DMSO was taken as blank. The cell viability was calculated by below equation 6.4.

$$\%Cell\ Viability = \frac{O.D._{.sample} - O.D._{.blank}}{O.D._{.negative\ control} - O.D._{.blank}} \times 100 \ldots\ldots\ldots\ldots\ldots 6.4$$

6.2.8.2. MCF-7 cell line:

The cell viability study was carried out on human breast carcinoma cell line *i.e.* MCF-7 for drug free and drug loaded nanoparticles. The MTT assay was initiated with the seeding step. The MCF-7 cells were seeded in the 96 well plate supplemented with DMEM containing sodium pyruvate, L-glutamate, sodium bicarbonate along with high glucose supplemented with 10% foetal bovine serum (FBS) and 1% penicillin-streptomycin (Pen/strep) solution which resists bacterial growth. For this, the 100µL cell suspension (10000 cells/well) was added to each well and incubated for 24 h at 37 ºC. The second step of the MTT assay was drug treatment. Here, BXR loaded nanoparticles containing 1-8µM equivalent BXR and drug free nanoparticles in the range of 0.1-100 µM were added and eventually well plate was incubated for a desired period time (24h and 72h). After the completion of desired time period, the MTT dye treatment was given and the well plate was read at 570nm. Here, the cells without

nanoparticle treatment was taken as a negative control and DMSO was taken as blank. Eventually, the %cell viability was calculated using the following equation 6.5.

$$\%Cell\ Viability = \frac{O.D._{.sample} - O.D._{.blank}}{O.D._{.negative\ control} - O.D._{.blank}} \times 100 \ldots\ldots\ldots\ldots\ldots 6.5$$

6.2.9. Cell permeability across Caco-2 cell monolayer:

It is an important task to determine the cell permeability of formulated nanoparticles, the Caco-2 cells were grown on the Trans well® inserts (Nunc, Denmark) having 0.4µ pore diameter with 1.13 cm^2 area. The inserts were thoroughly washed with the transport solution *i.e.* Hank's balanced salt solution (HBSS) containing 25mM of HEPES, pH 7.4. The integrity of the Caco-2 cells monolayer was tested by monitoring the Lucifer yellow dye permeability across the cell layer. Time dependent transport of BXR loaded nanoparticles was performed in unidirectional manner *i.e.* apical-to-basal. For this study, the donor compartment *i.e.* the apical side is treated with 0.5 mL of transport solution *i.e.* 1.5 M HBSS containing 0.1 mg/mL BXR and basal side was treated with 1.5 mL of HBSS solution. After incubation of 30, 60, 90, 120, 180, and 240 min, 100µL aliquots were withdrawn from the receiver and replenished with the equal volume of fresh HBSS. The samples were analysed by HPLC. The apparent permeability coefficient (P_{app}) was measured using the following equation.

$$P_{app} = \frac{dQ/dt}{A \times C_0} * 60 \ldots\ldots\ldots\ldots\ldots 6.6$$

Where, P_{app}: Apparent permeability coefficient (cm/h)

dQ/dt: drug permeation rate (mg/min)

A: cross-sectional area *i.e.* 1.13 cm^2

C_0: Initial BXR concentration in the donor compartment (mg/mL)

6.2.10. In vitro cellular uptake study:

6.2.10.1. Synthesis of FITC labelled nanoparticles:

The surface silanol group of bare nanoparticles was replaced with amine group using APTES. Now, this amine group would be available for the attachment of FITC molecule. The nanoparticle were labelled as per the procedures adopted earlier with slight modifications (20, 21) For this, a methanolic solution of FITC (0.3 mg/mL) was used. In which, the 10 mg aminated MSNs and HA@MSNs were added and exposed to continuous stirring in the darkness for 12h. Furthermore, the solution was centrifuged and washed with methanol for

complete removal of unconjugated FITC until the supernatants obtained were rendered colourless.

6.2.10.2. Intra cellular uptake study by confocal analysis:

Qualitative uptake of nanoparticles by MCF-7 cells was studied by confocal analysis. The MCF-7 cells were seeded in the 6 well plates containing coverslips ($5x10^5$ cells/well) one day before the drug treatment. Afterwards the cells were treated with the fixed concentration of FITC labelled MCM-NH_2-41, MCM-HA-41, HA+ MCM-HA-41 and MCM-NH_2-48, MCM-HA-48, HA+ MCM-HA-48 nanoparticles for 24h. After completion of the predefined time, the coverslips were washed thoroughly with the PBS and fixed with 3% paraformaldehyde for 5 min at room temperature and stained with DAPI followed by microscopical analysis on a Leica confocal microscope (22).

6.2.10.3. Intracellular uptake study by flow cytometry:

Flow cytometric analysis is an ideal approach for the quantification of internalization of nanoparticles. The experiment was initiated following seeding step. Here, cells ($5x10^5$ cells/well) were seeded in 12-well plate and incubated at 37 ºC for 24 h. Once the sufficient confluency is reached, the wells were treated with FITC labelled MCM-NH_2-41, MCM-HA-41, HA+ MCM-HA-41 and MCM-NH_2-48, MCM-HA-48, HA+ MCM-HA-48 nanoparticles and incubated at 37 ºC for 24 h. Afterwards, the cells were detached by trypsinization step. The cells were centrifuged at 1000 rpm for 3-5 min and the cell pellet was resuspended in FACS buffer by aspirating through pipetting and vortexing it to carry out the uptake study on FACS Calibur flow cytometer. All the experiments were carried out in triplicate. Here the untreated cells were taken as control.

(FACS buffer preparation: 0.5 gm bovine serum albumin and 0.5 mL FBS were mixed together and volume was made to 100 mL by PBS solution)

6.2.11. Apoptosis assay

Annexin V-FITC double stain apoptosis detection kit from BD Biosciences was used for study. The MCF-7 cells were seeded at a density of $5x10^5$ cells/well and incubated for 24 h and. The cells were given PBS wash for twice and subsequently, treated with BXR, BXR-HA-41 and BXR-HA-48 nanoparticles at their respective concentrations (5µM). This was followed by cold PBS (4°C) wash after 24 h and stained with FITC-Annexin V. Concisely, the cells were suspended in 1 mL of 1 × binding buffer at a concentration of 1×10^5 cells/mL. Further, 5µL

of FITC-Annexin V and 5µL of PI were added per 100µL of the suspension (1×10^5). After mild vortexing, the cells were incubated for 15 min in the dark. Finally, 400 µL of 1 × binding buffer was added to each tube and analysed by flow cytometry.

6.2.12. Hemolysis study:

It is very essential to study the compatibility of formulated nanoparticles with the erythrocytes (23). Hence, the hemolysis study was performed as per the literature method for engineered parenteral formulations. (24-26). The freshly collected blood sample was centrifuged at 8000 rpm for 5 min at 4 ºC. The plasma supernatant was removed and the residue was washed with PBS buffer (pH: 7.4) and diluted 10 folds. To the 200 µL RBC solution, 800 µL of nanoparticle solution (BXR, BXR-HA-41 and BXR-HA-48) having the concentration of 0.1-100 µg/mL were prepared individually. The few drops of the sample were plated on the glass slide and analyzed by the microscope. Additionally, for the quantitative analysis, all the samples were incubated for 2 h at 37 ºC and centrifuged at 10000 rpm for 2 min at 4 ºC and the collected supernatant was analyzed by UV-VIS spectrophotometer at 570 nm. Eventually, the %hemolytic activity was calculated considering following formula. 2%v/v Triton X_{100} was taken as a positive control and PBS buffer (pH: 7.4) was taken as a negative control respectively.

$$\%Hemolysis = \frac{A_{sample} - A_{Negative\ Control}}{A_{Positive\ Contol} - A_{negative\ Contol}} \times 100 \ldots\ldots\ldots\ldots\ldots 6.7$$

6.2.13. In vivo pharmacokinetic study:

6.2.13.1. Pharmacokinetic study for oral formulation:

6.2.13.1.1. Experimental:

Female Swiss albino mice were housed in a ventilated cage and given free access to food and water and acclimatized for a week before performing the actual experiment. The animals were divided into a group of 7 and each group containing 3 animals and they were fasted overnight and given free access to water for 12 hours before giving the first dose. Group-I animals were labelled as controlled group and they were given 0.9% w/v saline solution (negative control). Group-II animals were given BXR suspension prepared in saline solution having dose equivalent to 7.4mg/kg were administered. Similarly, group-III, group-IV, group-V, group-VI and group-VII was given marketed formulation, BXR-41, BXR-48, BXR-NH_2-41, and BXR-NH_2-48 (each equivalent to 7.4mg/kg BXR) respectively. All the formulation was administered using syringes and infant feeding tube. The blood samples were withdrawn using a capillary

tube at 0.5, 1, 2, 4, 8 and 12h post dosing from the retro-orbital venous plexus and collected in the EDTA treated tubes.

6.2.13.1.2. Sample preparation:

The protein precipitation method was optimized to recover the sample from the bioanalytical matrix. Briefly, the collected blood samples were centrifuged at 5000 rpm for 10 min at 4 ºC temperature and plasma was collected. To the 100µL of the plasma sample, 50 µL of internal standard (Clopidogrel: 10 ppm) was incorporated and vortexed for 1 min. furthermore, 300 µL of ACN was added and vortexed for 3 min. Thereafter, the reaction assembly was centrifuged at the 5000 rpm for 10 min keeping 4 ºC temperature. 10 µL of the supernatant was removed and analysed by HPLC.

6.2.13.1.3. Pharmacokinetic parameters evaluation:

Different pharmacokinetic parameters were calculated from the plasma concentration time data by means of a model independent method *i.e.* non-compartmental model using PK solver software®. Peak plasma concentration (C_{max}), $T_{1/2}$ and time required to achieve C_{max} *i.e.* t_{max} were obtained by visual inspection of the experimental data. Moreover, the linear trapezoidal method was applied to determine area under curve (AUC_{0-t}).

6.2.13.2. Pharmacokinetic study for parenteral formulation:

For pharmacokinetic study of the parenteral formulation, a total of 12 mice were randomly divided into 3 groups (n=4) and intravenously injected saline, BXR, BXR-HA-41 and BXR-HA-48 from the tail vein with a 0.5 CC U40 insulin syringe fitted with a 28-$g^{1/2}$. The blood sample (0.3 ml) was collected at specific time intervals and stored in EDTA added centrifuge vials. Further, plasma was separated by centrifugation at 4000 rpm for 10 minutes at 4°C. 100µL plasma was mixed with internal standard CLOPI. The samples were precipitated by adding Acetonitrile (ACN) and again centrifuged at 5000 rpm for 10 min. The supernatants were collected and BXR was quantified using a HPLC. Different pharmacokinetic parameters viz C_{max}, T_{max} and AUC were calculated by using PK Solver excel add-in.

6.2.14. In vivo biodistribution study and histological examination

The biodistribution of formulated final nanoparticles in major organs was studied following parenteral administration of BXR, BXR-HA-41 and BXR-HA-48 in the mice. Sterile saline injections at equivalent volumes were given to mice as control. Mice were sacrificed at 24 h after injection and major organs like heart, liver, lung, kidney, prostate, brain and spleen were collected and weighed. Furthermore, PBS solution was added to each tissue sample by an equal

volume to its weight and subjected to high speed homogenization. The mixtures obtained were centrifuged at 10000 rpm for 10 min. The supernatant was collected and extracted with ACN. The extracted sample was analyzed and quantified by HPLC to report the concentration of BXR in different organs.

The aforementioned major organs collected were fixed in 10% formalin in PBS solution. The organs were embedded in paraffin and sectioned to 4µm sections and placed onto the glass slides. The histological sections were stained with H&E and observed under microscope.

6.2.15. Statistical analysis

The experiments were conducted thrice, and the results were expressed as the means and standard deviations from the triplicate experiments unless mentioned otherwise. The statistical analysis was performed by one-way ANOVA and p-values less than 0.05 were considered as significant.

6.2.16. Stability study of prepared nanoparticles:

The stability study of synthesized nanoparticles *i.e.* BXR-41, BXR-NH_2-41, BXR-HA-41, and BXR-48, BXR-NH_2-48, BXR-HA-48 were performed as specified in ICH Q1A(R2). The synthesized nanoparticles were exposed to 40±2 ºC and 75±5 %RH conditions and sampling was done at 0^{th} day, 3^{rd} month and 6^{th} month and samples were analyzed by DSC and SXRD.

6.3. Result and discussion:

6.3.1. Solid state evaluation of MSNs:

6.3.1.1. FTIR:

Characterization of formulated nanoparticles was initiated with the preliminary FTIR investigation. FTIR is an essential qualitative technique for affirming the MSNs synthesis, BXR uptake by MSNs and amine grafting on the surface of MSNs as well. Figure 6.1 represents a characteristic FTIR vibrational peak due to mesoporous assembly for MCM-41 and surface decorated MCM-41 type of nanoparticles. Figure 6.1A demonstrates a broad –OH stretching peak, a shoulder peal due to $–CH_2$ group, C=O stretching peak and peak due to –CONH group at 3200-3600 cm^{-1}, 2900 cm^{-1}, 1100-1300 cm^{-1}, 16600-1650 cm^{-1} respectively for pure HA. Figure 6.1B demonstrated a prominent IR peaks at 2922 and 2852 cm^{-1} due to C-H stretching vibration and C-H deformation vibration peak at 1454 cm^{-1} could be accredited to template moiety occupied in the mesopores of CTAB@MCM-41. The success of the formation of MCM-41 can be confirmed by assigning presence of the fingerprint IR vibration peaks at 1100 and 780 cm^{-1} wavenumbers due to symmetric and asymmetric stretching of Si-O-Si respectively in figure 6.1B. Additional blunt and diffused stretching vibrational peak over the region of 3300-3500 cm^{-1} indicates the presence of terminal Si-OH (silanol) group. Furthermore, disappearance of representative C-H stretching peak also supports the hypothesis of removal of surfactant after calcination (figure 6.1C). The favourable output of amine grafting on the external surface was gathered from the N-H bending peak and C-H stretching peak at 1585 cm^{-1} and 2915 cm^{-1} respectively for MCM-NH_2-41 as portrayed in figure 6.1D. On the other hand, the MCM-HA-41 exhibits a typical FTIR peaks due to O-H, C-H stretching, and Si-O-Si stretching in the region of 3379, 2907, and 1060 cm−1 respectively in figure 6.1E is assigned to HA grafting on MCM-HA-41.

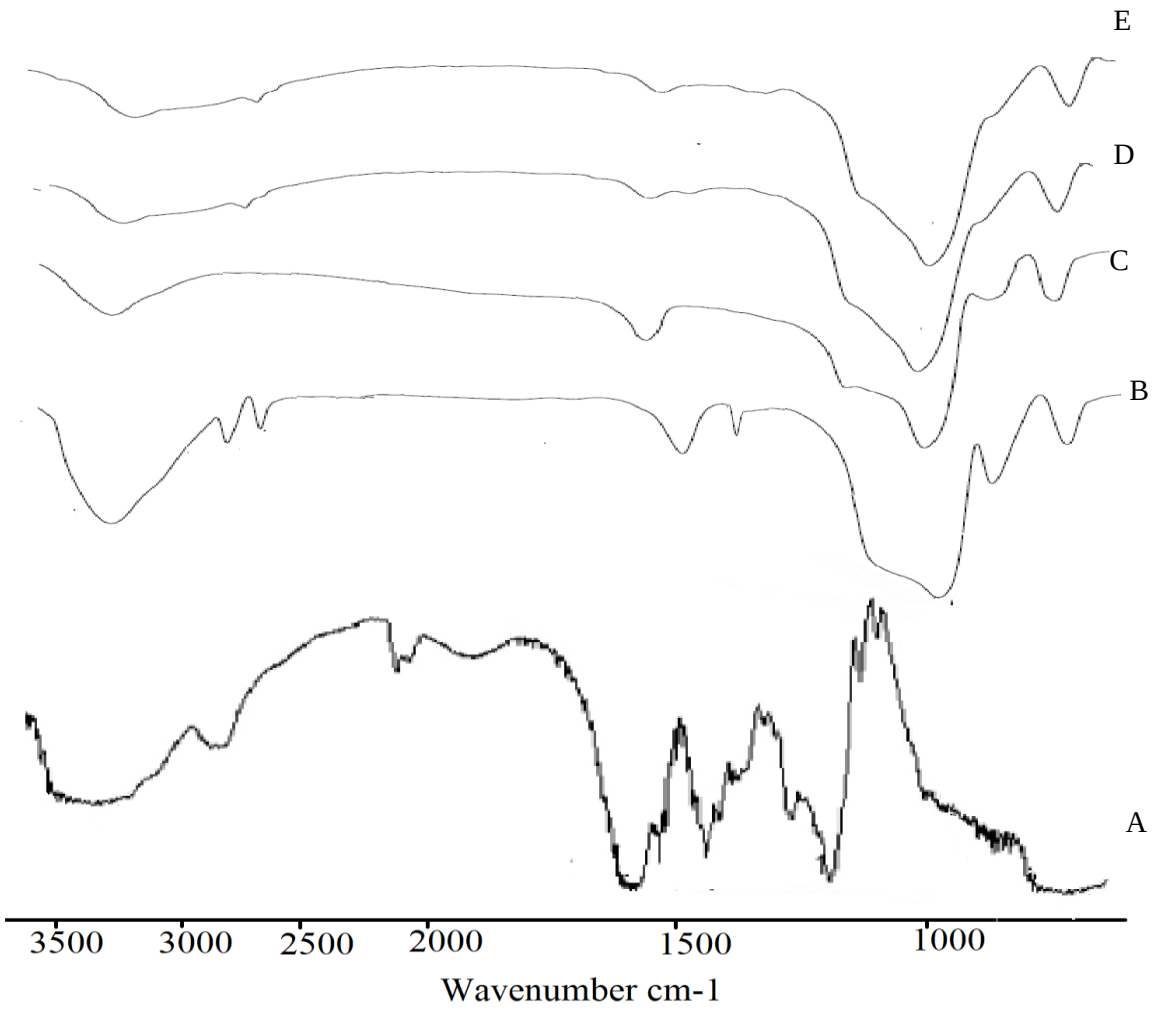

Figure 6.1. FTIR spectra of (A) HA, (B) CTAB@MCM-41, (C) MCM-41, (D) MCM-NH_2-41, (E) MCM-HA-41

Figure 6.2 demonstrated a FTIR spectra of BXR loaded MCM-41 type of nanoparticles. Figure 6.2A displayed a characteristic functional group peaks for BXR at 1720 cm^{-1} and 2875 cm^{-1} is corresponded to C=O group and the C-H group present in the moiety respectively. Besides, the bands encountered at 1480 and 1431 cm^{-1} could be accredited to C=C stretching present in the phenyl backbone of the aromatic ring. Nonexistence of BXR symbolic peaks for BXR-41, BXR-NH_2-41, and BXR-HA-41 emphasizes BXR uptake by MCM-41 (figure 6.2B), MCM-NH_2-41 (figure 6.2C), and MCM-HA-41(figure 6.2D) respectively.

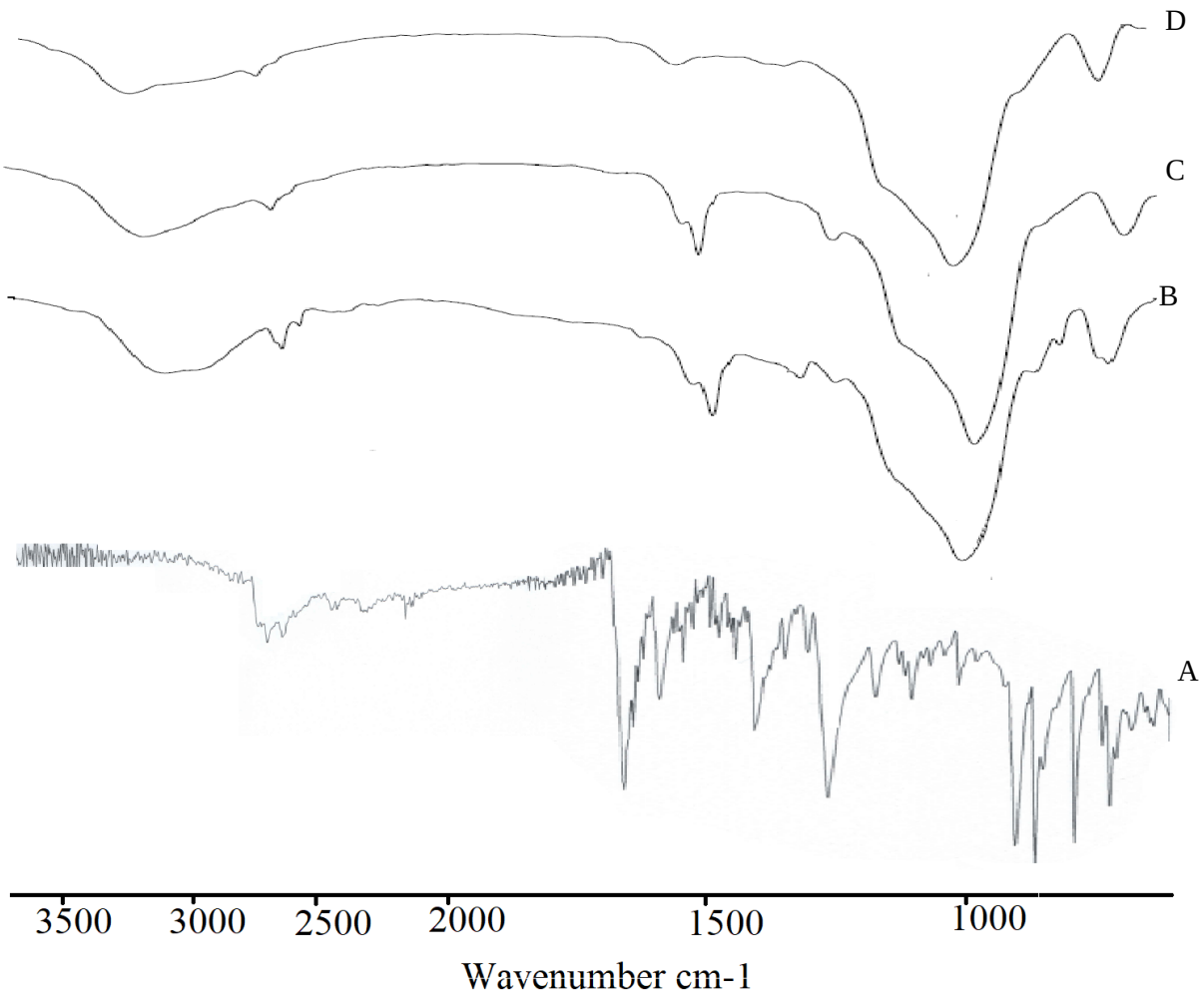

Figure 6.2 FTIR spectra of (A) BXR, (B) BXR-41, (C) BXR-NH_2-41 and (D) BXR-HA-41

Similar outcomes for pristine and surface coated MCM-48 type nanoparticles revealed successful grafting of organic moieties along with formation of mesoporous assembly (figure 6.3). Additionally, the FTIR spectra of BXR loaded nanoparticle demonstrated complete encapsulation of BXR inside the MCM-48 type of nanoparticles (figure 6.4).

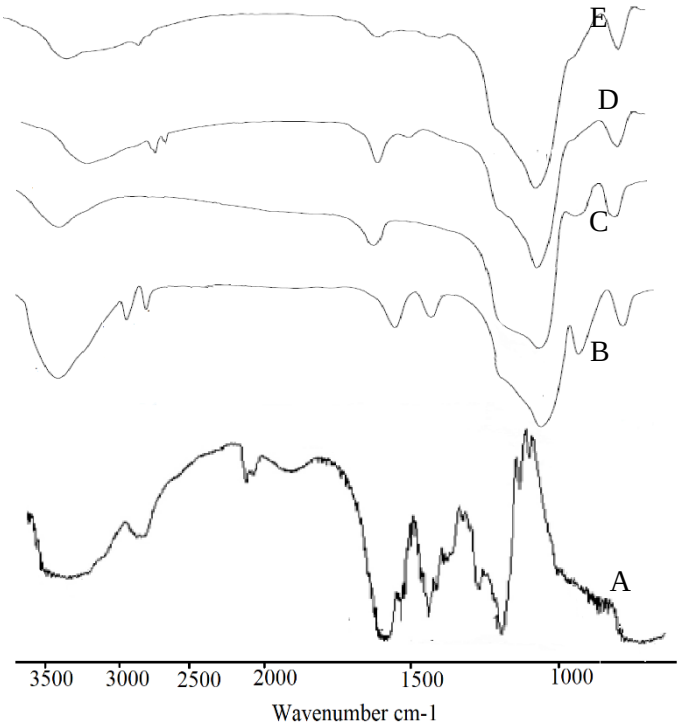

Figure 6.3 FTIR spectra of (A) HA, (B) CTAB@MCM-48, (C) MCM-48, (D) MCM-NH_2-48, (E) MCM-HA-48

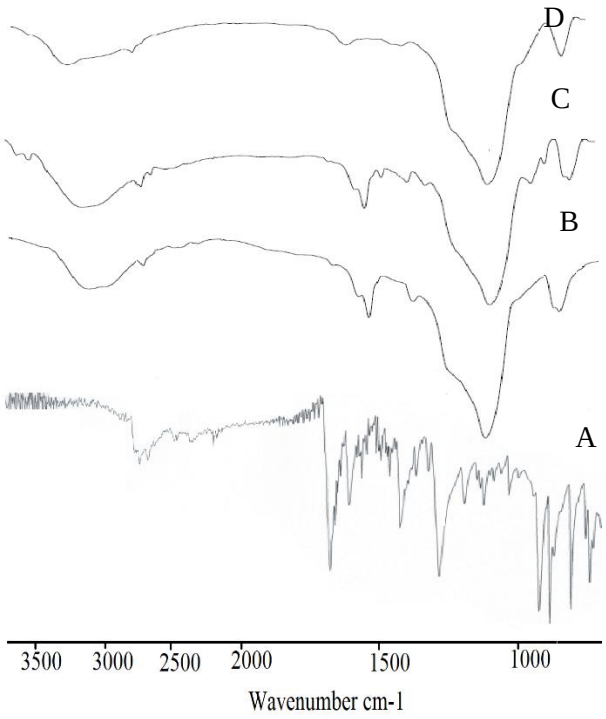

Figure 6.4. FTIR spectra of (A) BXR, (B) BXR-48, (C) BXR-NH_2-48 and (D) BXR-HA-48

6.3.1.2. DSC:

DSC thermogram of plain BXR along with BXR-41, BXR-NH_2-41 and BXR-HA-41 is illustrated in figure 6.5A-D. Figure 6.5A represented a solitary endothermic peak at 225.55 ºC which could be corresponded to BXR melting point. Identical outcome was acquired for BXR loaded MCM-41, MCM-NH_2-41 and MCM-HA-41 wherein, the typical endothermic peak at 225.55 ºC owed to BXR melting was missing, which strongly suggest a change in the nature of BXR *i.e.* from crystalline to non-crystalline subsequent to complete incorporation inside the pores. Furthermore, this result was in synchronization with that acquired FTIR study as discussed earlier.

Similar results were obtained for bare and surface coated MCM-48 type of nanoparticles as portrayed in figure 6.6A-D. Thus, the BXR was successfully encapsulate within the MCM-48 types of mesoporous carrier also.

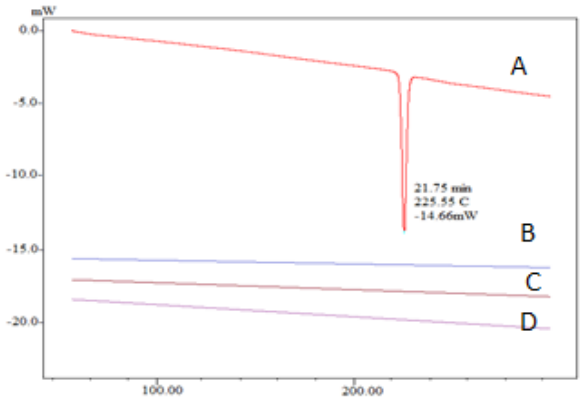

Figure 6.5: DSC thermogram of (A) BXR, (B) BXR-41, (C) BXR-NH$_2$-41, (D) BXR-HA-41

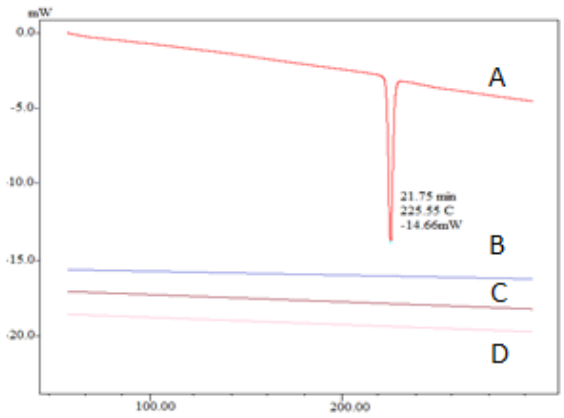

Figure 6.6: DSC thermogram of (A) BXR, (B) BXR-48, (C) BXR-NH$_2$-48, (D) BXR-HA-48

6.3.1.3. WXRD:

Similar conclusion regarding drug uptake was established through WXRD study. The WXRD spectra ranging from 10º to 40º 2θ/º region is represented in below figures. Where, figure 6.7A revealed few indicative peaks for pure BXR which were lacking in the BXR incorporated MCM-41 and MCM-48 type nanoparticles as shown in figure 6.7B-D and figure 6.8B-D respectively.

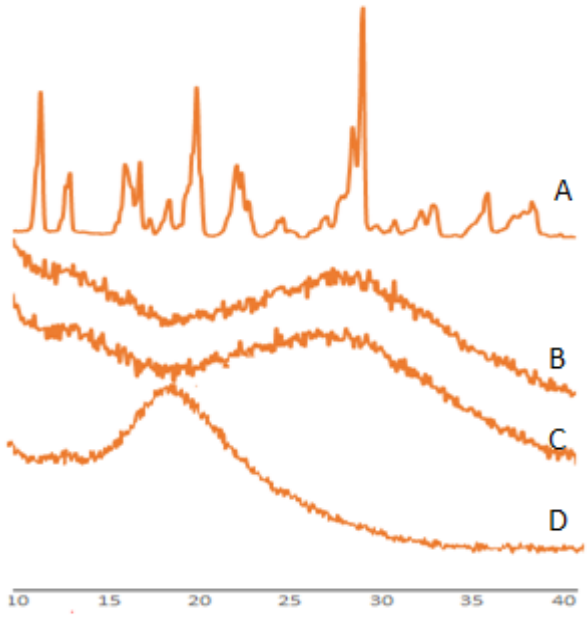

Figure 6.7: WXRD spectra of (A) BXR, (B) BXR-41, (C) BXR-NH$_2$-41 and (D) BXR-HA-41

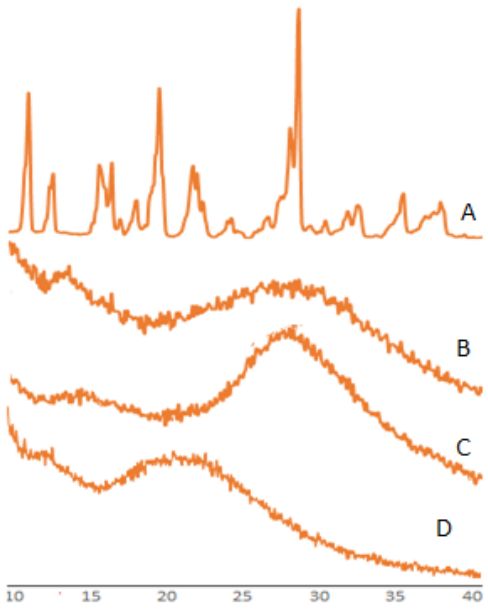

Figure 6.8: WXRD spectra of (A) BXR, (B) BXR-48, (C) BXR-NH$_2$-48, and (D) BXR-HA-48

6.3.1.4. SXRD:

The surface functionalization and BXR impregnation by bare and surface coated NPs were confirmed by SXRD. Apart from giving aforementioned information, SXRD also utilized as an evidence to demonstrate the persistence of mesoporous integrity after surface capping and BXR uptake as well. The mesoporous skeleton for MCM-41 and MCM-48 were affirmed by the typical SXRD peaks in the region of 1º to 10º 2θ/º. Concisely three distinct peaks were identified at 100, 110 and 200 2θ/º attributed to the mesoporous assembly of MCM-41 as illustrated in figure 6.9A. Moreover, the peak at 100 2θ/º obtained for MCM-NH_2-41 and MCM-HA-41 demonstrates noteworthy reduction in the intensity which strongly suggests amine and HA grafting (figure 6.9B and 6.9C). Furthermore, a surface coating might be responsible to a drastic reduction in the intensity of the peaks which ultimately accounted for the disappearance of two successive peaks at 110 and 200 for surface coated nanoparticles.

Similar results were encountered for BXR-41, BXR-NH_2-41 and BXR-HA-41 (figure 6.10A-C) with a reduction in the intensity compared to drug free nanoparticles which could be due to BXR encapsulation inside the pores.

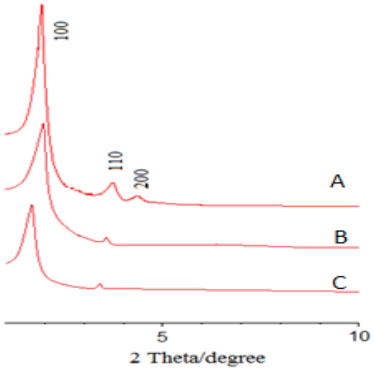

Figure 6.9: SXRD spectra of (A) MCM-41, (B) MCM-NH_2-41 and (C) MCM-HA-41

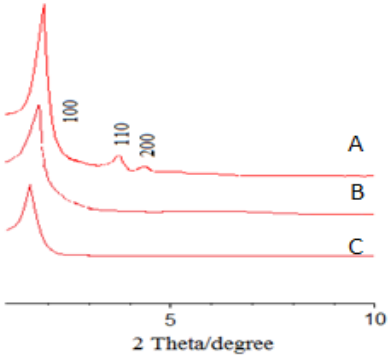

Figure 6.10: SXRD spectra of (A) BXR-41, (B) BXR-NH_2-41 and (C) BXR-HA-41

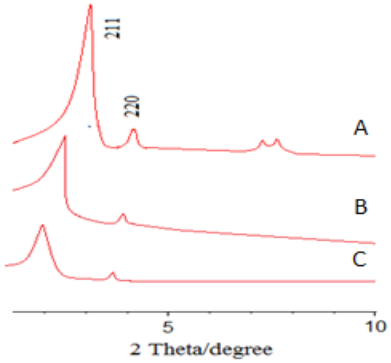

Figure 6.11: SXRD spectra of (A) MCM-48, (B) MCM-NH_2-48 and (C) MCM-HA-48

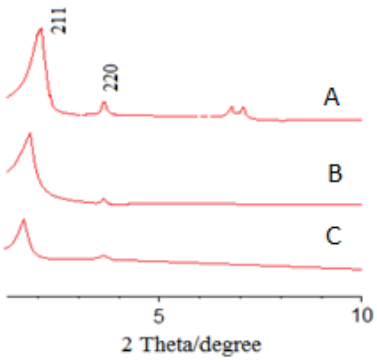

Figure 6.12: SXRD spectra of (A) BXR-48, (B) BXR-NH_2-48 and (C) BXR-HA-48

On the other hand, figure 6.11A exemplified two peaks at 211, 220 and other two peaks at the higher side for MCM-48. These aforementioned peaks existed for MCM-NH_2-48 and MCM-HA-48 with reduced intensity which again emphasizes the formation of functionalized nanoframework (figure 6.11B and 6.11C). Additionally, the reduction in the intensity of drug loaded nanoparticles with respect to BXR free nanoparticles ascertained complete BXR loading within the mesopores without distortion of the mesoporous skeleton (figure 6.12A-C).

6.3.1.5. Nitrogen sorption study:

Furthermore, the type IV isotherm with the hysteresis loop for formulated nano assembly were acquired through comprehensive BET analysis. BET investigation demonstrated higher surface area with the optimized pore size which might have greater influence in the dissolution and in turn bioavailability enhancement. The nitrogen desorption analysis outcomes revealed a significantly higher BJH surface area for bare and drug free MSNs *i.e.* 578.15 m^2/g. The same parameter showed gradual decline in the value after surface modification by amine and HA group *i.e.* 352.14 m^2/g and 239.63 m^2/g respectively (figure 6.13A-C). BET surface area for BXR-41 were 375.34 m^2/g and decline after drug loading (figure 6.14A-C). Identical investigation was carried out for MCM-48 also, where the surface area of bare nanoparticle was decreased from 840.54 m^2/g to 274.49 m^2/g for final formulation (figure 5.15A-D and 5.16A-D). The data gathered were portrayed in figure 6.15 and figure 6.16 for BXR free, and BXR encapsulated nanoparticles respectively. Besides these, pore size distribution and pore volume data were also gathered for all varied kinds of nanoparticles as summarized in table 6.3 and also depicted in figure 6.17 for BXR loaded and unloaded MCM-41. The similar information is given in figure 6.18 and table 6.4 for MCM-48. Wherein, a sharp rise in the pore volume at a single point (due to capillary condensation of nitrogen) unveiled uniform pore size distribution of formulated mesoporous system.

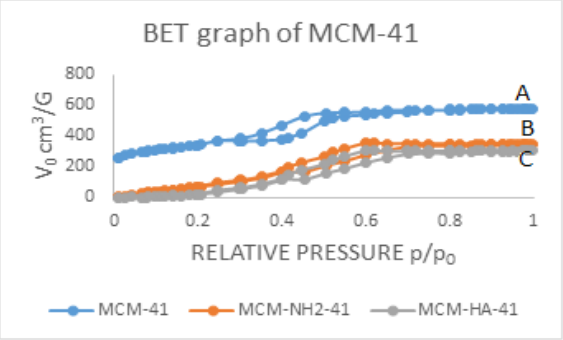

Figure 6.13 BET graph of (A) MCM-41, (B) MCM-NH_2-41 and (C) MCM-HA-41

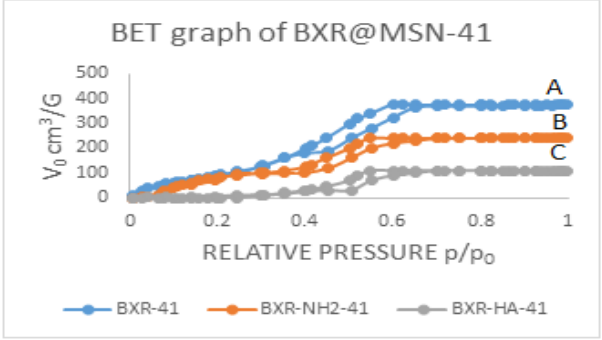

Figure 6.14: BET graph of (A) BXR-41, (B) BXR-NH_2-41 and (C) BXR-HA-41

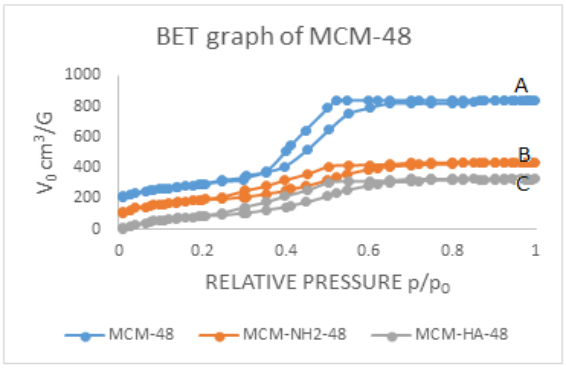

Figure 6.15: BET graph of (A) MCM-48, (B) MCM-NH$_2$-48 and (C) MCM-HA-48

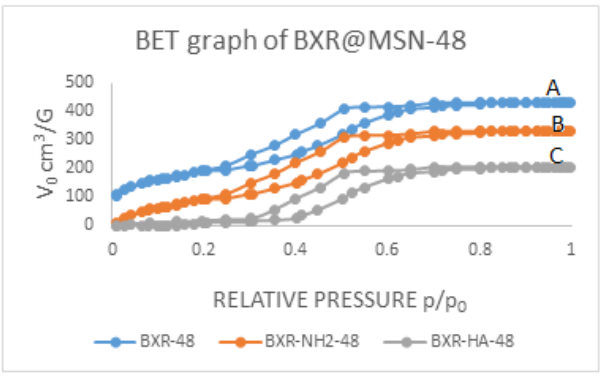

Figure 6.16: BET graph of (A) BXR-48, (B) BXR-NH$_2$-48 and (C) BXR-HA-48

(A) (B) (C)

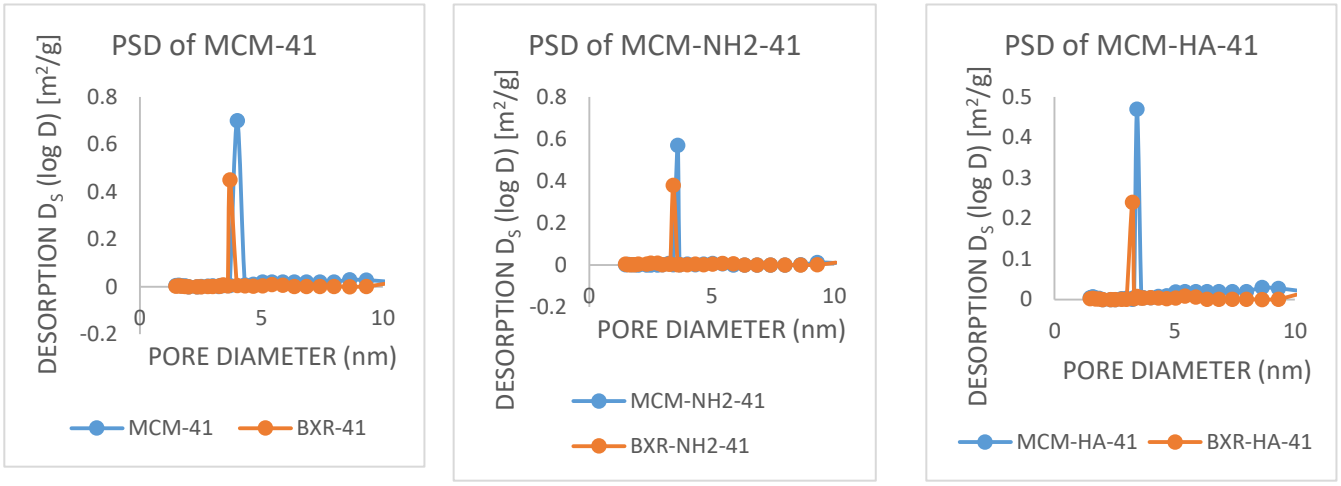

Figure 6.17: PSD graph for drug free and drug loaded (A) MCM-41, (B) MCM-NH$_2$-41 and (C) MCM-HA-41

Table 6.3: BET and ZETA characteristics for bare and surface coated MCM-41

Sample name	BET surface area (m²/g)	BJH surface area (m²/g)	Pore size (nm)	Pore volume (cm³/g)	Hydrodynamic size (nm)	Zeta potential (mV)
MCM-41	578.17	710.94	4.01	0.72	95	-24.82
BXR-41	375.34	461.25	3.72	0.45	-	-30.41
MCM-NH$_2$-41	352.24	432.96	3.61	0.57	108	+26.75
BXR-NH$_2$-41	240.71	295.27	3.43	0.38	-	+20.67
MCM-HA-41	239.54	292.66	3.43	0.47	124	-18.64
BXR-HA-41	144.27	196.47	3.24	0.24	-	-28.77

(A) (B) (C)

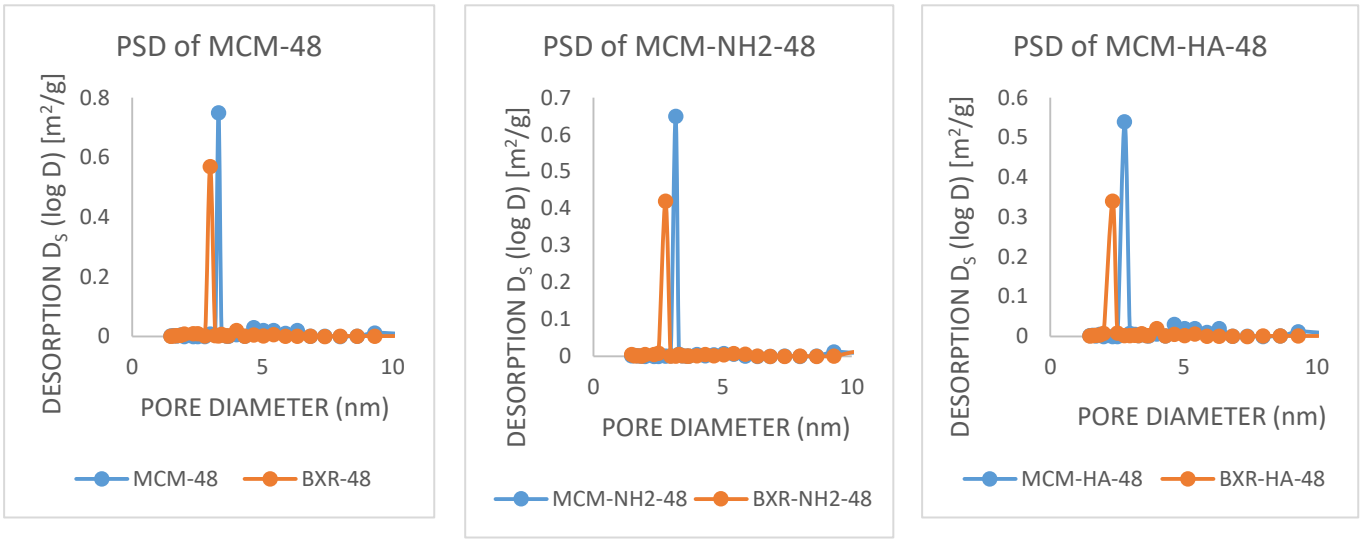

Figure 6.18: PSD graph for (A) MCM-48, (B) MCM-NH_2-48 and (C) MCM-HA-48

Table 6.4: BET and ZETA characteristics for bare and surface coated MCM-48

Sample name	BET surface area (m^2/g)	BJH surface area (m^2/g)	Pore size (nm)	Pore volume (cm^3/g)	Hydrodynamic size (nm)	Zeta potential (mV)
MCM-48	840.54	1033.21	3.35	0.75	83	-30.17
BXR-48	512.03	629.76	2.99	0.57	-	-36.24
MCM-NH_2-48	432.61	531.36	3.18	0.65	98	+31.88
BXR-NH_2-48	332.27	408.36	2.79	0.42	-	+26.37
MCM-HA-48	274.49	381.25	2.79	0.54	115	-21.68
BXR-HA-48	203.68	315.34	2.34	0.34	-	-32.07

6.3.1.6. DLS study:

The surface charge for the pristine MCM-41 particles remain positive due to presence of abundant silanol group on the outer surface. The shifting of the zeta potential of MCM-41 from negative side (-24.82) to a positive value (+26.75) is due to the presence of an amine group on the surface of MCM-NH_2-41. Whereas, in case of MCM-HA-41 the potential value shifted toward lower side *i.e.* from +26.75 mV to -18.64 due to HA moiety. Further, it is essential to notice a constant negative shifting in zeta potential value after BXR uptake as compared to unfilled nanoparticles. This observation concludes that the BXR moiety might have positively charged surface which could be responsible in the enhancement of the potential after drug encapsulation (table 6.3). Additionally, the particle size readings were also acquired from DLS

study, which revealed formation of monodispersed nanoparticles in the range of 90-150 nm with successive increment with the coating. The similar zeta potential pattern was observed for BXR free and BXR filled MCM-48 nanoparticles and the outcomes are listed in the table 6.4.

6.3.1.7. SEM and TEM analysis:

The uniformity in the particle size and shape were asserted following SEM and TEM data. Figure 6.19 and figure 6.20 illustrated SEM images for bare and surface coated MCM-41 and MCM-48 nanoparticles which displayed a uniform spherical shape of MSNs. The further idea regarding the particle size were obtained from the SEM analysis. The 2D hexagonal and 3D cubic mesoporous frameworks for MCM-41 and MCM-48 nanoparticle respectively were revealed from TEM analysis. The mesoporous skeleton was remained undisturbed even after surface coating also which could be inferred from the TEM inspection of surface decorated nanoparticles. Figure 6.21 and figure 6.22 revealed a TEM images for synthesized bare and surface modified nanoparticles for MCM-41 and MCM-48 respectively. Where, figure 6.21 is corresponding to the 2D hexagonal honeycomb assembly of MCM-41. Whereas, the 3D cubic channel observed for MCM-48 is clearly observed in the respective figure 6.22. The results demonstrated an undisturbed internal 2D hexagonal and 3D cubic skeleton even after surface modification.

(A) (B) (C)

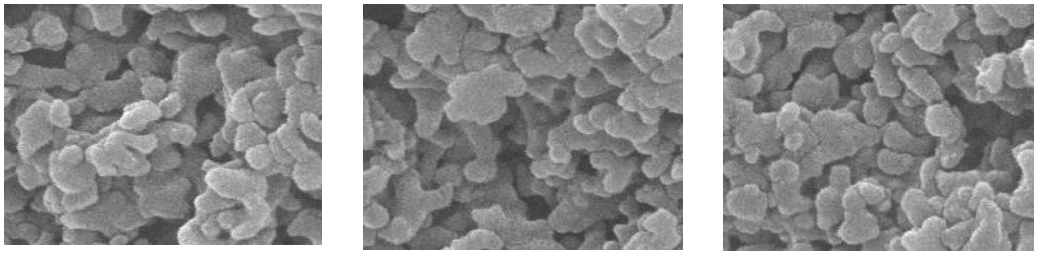

Figure 6.19: SEM images for (A) MCM-41, (B) MCM-NH_2-41 and (C) MCM-HA-41

(A) (B) (C)

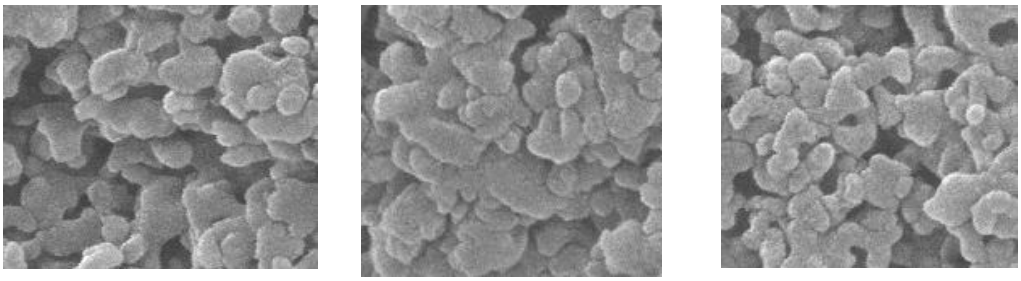

Figure 6.20: SEM images for (A) MCM-48, (B) MCM-NH_2-48 and (C) MCM-HA-48

(A) (B) (C)

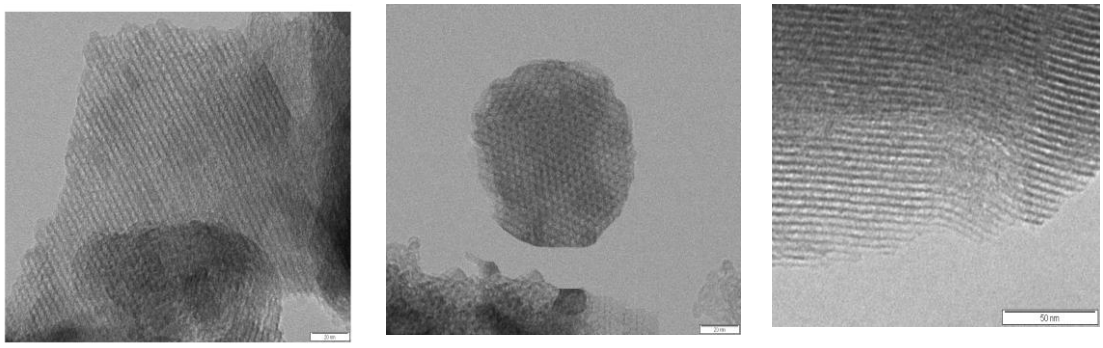

Figure 6.21: TEM images for (A) MCM-41, (B) MCM-NH_2-41 and (C) MCM-HA-41

(A) (B) (C)

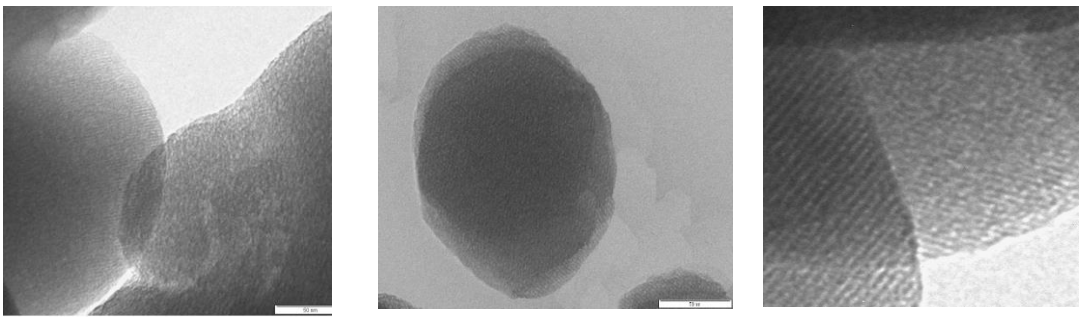

Figure 6.22: TEM images for (A) MCM-48, (B) MCM-NH_2-48 and (C) MCM-HA-48

6.3.2. Estimation of %loading efficiency and entrapment efficiency:

The BXR loaded nanoparticles were prepared using a novel immersion evaporation technique. As being a hydrophobic drug, BXR is having maximum solubility in organic solvent especially in MeOH. Therefore, during the drug loading, BXR was dissolved in MeOH and in this solubilized form, active drug molecule diffuses inside the mesopores through the capillaries and after solvent removal, drug remains entrapped inside the pores. Though confirmation of uptake by nanoparticles were accomplished through aforementioned different techniques, the extent of loading and entrapment for carrier and BXR respectively were still left to be determined. This investigation was conducted performing UV and TGA analysis of BXR engulfed nanoparticles. Information collected from both the techniques were complementary to each other as summarized in table 6.5.

The TGA curve of BXR displayed an expeditious fall initiated at near 200 ºC and lasted upto 300 ºC. This could be due to thermal decomposition of drug moiety (figure 6.23). The BXR thermogram showed complete decomposition of pure drug moiety with the 100 %weight loss. Further the %loading efficiency was calculated from the weight loss of the BXR assembled in nanosystem. TGA thermogram stated 36.06%, 38.66% and 34.86% BXR

encapsulation for BXR-41, BXR-NH_2-41 and BXR-HA-41 respectively. The reason for higher drug loading inside the positively charged MCM-NH_2-41 could be the electrostatic diffusion of negatively charged BXR inside the pores (figure 6.23). Furthermore, the loading results were promising for the MCM-48 NPs as compared to MCM-41 NPs. The result demonstrated a higher BXR encapsulation *i.e.* 38.02%, 39.86% and 36.17% for BXR-48, BXR-NH_2-48 and BXR-HA-48 successively (figure 6.24). Again, the reason for higher drug uptake by aminated NPs could be the same as mentioned earlier.

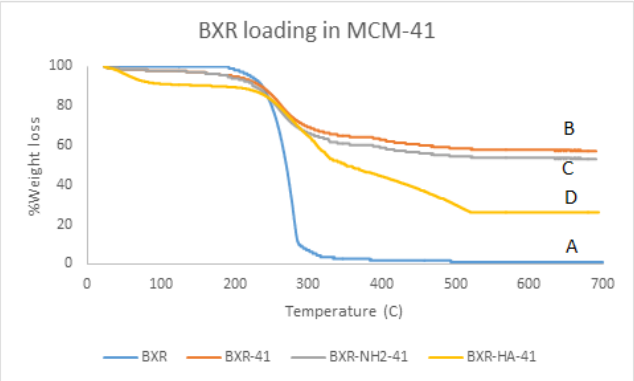

Figure 6.23: TGA thermogram for (A) BXR, (B) BXR-41, (C) BXR-NH_2-41 and (D) BXR-HA-41

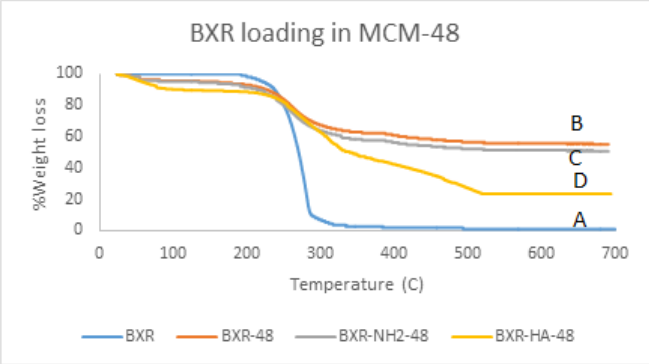

Figure 6.24: TGA thermogram for (A) BXR, (B) BXR-48, (C) BXR-NH_2-48 and (D) BXR-HA-48

Table 6.5: %Loading and %entrapment efficiency data of BXR

Sr No.	Formulation	D:C Ratio	% Loading		% Entrapment
			By UV	By TGA	
1.	BXR-41	1:1.5	36.15	36.06	92.56
2.	BXR-NH_2-41	1:1.5	38.86	38.66	96.65
3.	BXR-HA-41	1:1.5	35.37	34.86	87.15
4.	BXR-48	1:1.5	38.99	38.02	97.65
5.	BXR-NH_2-48	1:1.5	39.91	39.86	98.9
6.	BXR-HA-48	1:1.5	37.58	36.17	90.42

6.3.3. %Grafting of different surface modifying agents

The Ninhydrin colorimetric assay was performed and absorbance of Ninhydrin-primary amine complex was taken into consideration for the %amine grafting calculation. Colorimetric analysis of MCM-NH_2-41 and MCM-NH_2-48 at 590 nm showed 2.46% and 4.15% amine decoration respectively. The results were calculated applying equation 6.3-6.5.

TGA results are represented in terms of temperature dependent weight loss (27). Wherein the TGA graph was divided into two distinctive temperature range regions. The first region comprises of region of weight change between 20-150 °C. The weight loss occurred over this range of temperature could be solely accredited to the thermal desorption of surface water adsorbed physically over the silica surface. On the other hand, the second region comprised of weight change beyond 150°C temperature. A comparative flat TGA curve represents a negligible weight loss at the higher temperature. The minor change in the weight could be assigned to silanol condensation followed by siloxane bond formation (28). All the MSNs exhibited outstanding stability within the studied temperature range. Although the TGA curve for surface functionalized nanoparticles was easily distinguishable from that of bare silica thermogram especially in the second region of weight loss due to loss or decomposition of grafted moiety takes place beyond 150 ºC. The larger is the percentage weight loss, the higher would be extend of surface functionalization (29). Equations 6.6 were taken into consideration for the %amine grafting calculation by TGA and the results were in accordance to the outcome obtained from Ninhydrin colorimetric assay (figure 6.25 and 6.26). further the figure of %grafting for MCM-41 and MCM-48 is listed in table 6.6.

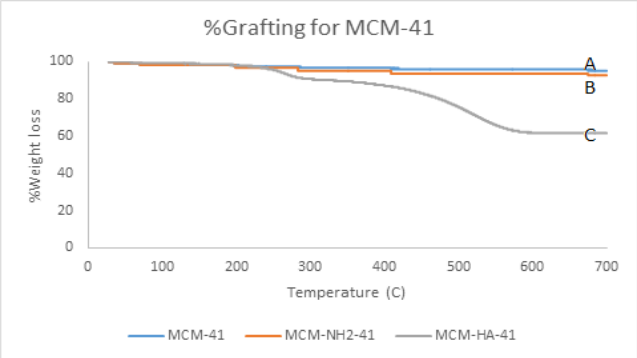

Figure 6.25: TGA thermogram of (A) MCM-41, (B) MCM-NH$_2$-41 and (C) MCM-HA-41

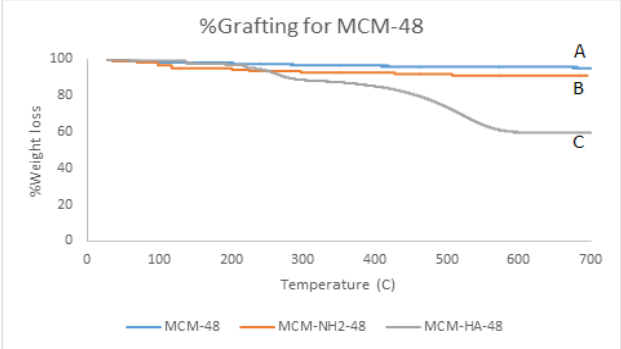

Figure 6.26: TGA thermogram of (A) MCM-48, (B) MCM-NH$_2$-48 and (C) MCM-HA-48

Table 6.6: %Weight grafting results

Sample Name	A_m (mol/g)	A_n (molecule/nm^2)	%W	
			Ninhydrin	TGA
MCM-NH$_2$-41	$0.55*10^{-3}$	0.39	2.57%	2.46%
MCM-HA-41	-	-	-	23.89
MCM-NH$_2$-48	$0.95*10^{-3}$	0.18	4.29%	4.15%
MCM-HA-48	-	-	-	25.73

Besides this, the elemental detection for each nanoparticles by SEM-EDX. The outcomes revealed presence of Si and Oxygen elements in the bare MSNs whereas, the extra peak due to nitrogen and carbon were encountered in the MCM-NH_2-41 and MCM-HA-41 (figure 6.27) as well for MCM-NH_2-48 and MCM-HA-48 (figure 6.28) confirmed the success of amine and HA coating on the exterior.

(A)

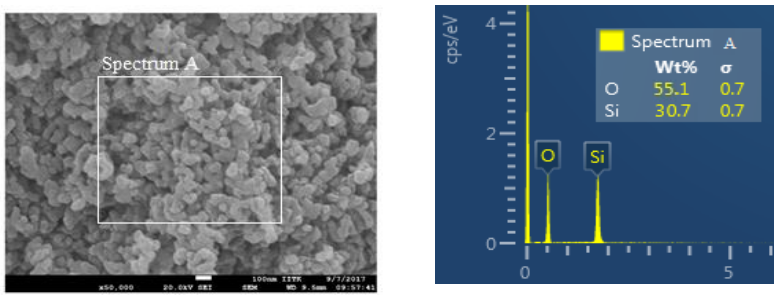

(B)

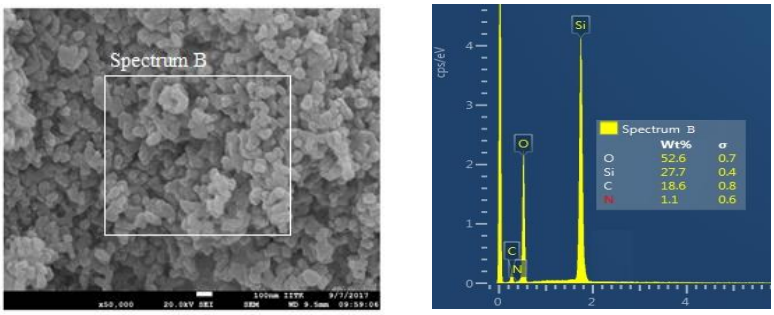

(C)

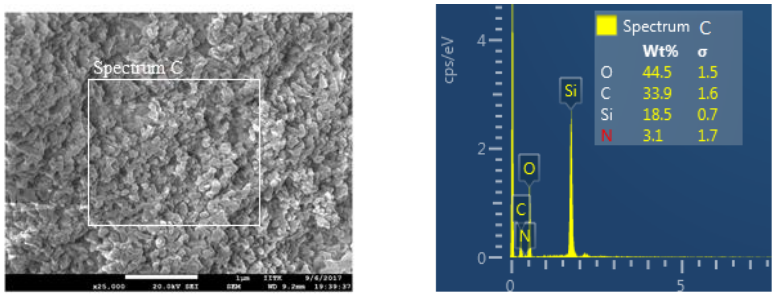

Figure 6.27: SEM-EDX images for (A) MCM-41, (B) MCM-NH_2 -41 and (C) MCM-HA-41

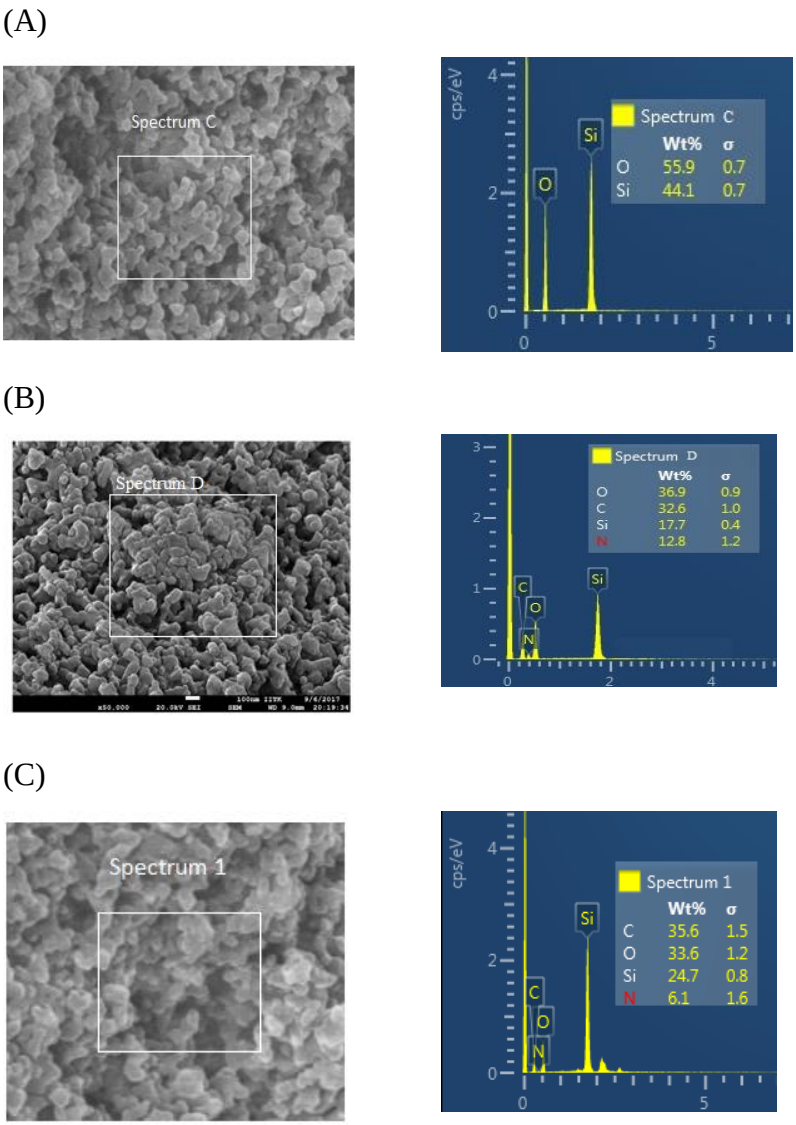

Figure 6.28: SEM-EDX images for (A) MCM-48, (B) MCM-NH_2 -48 and (C) MCM-HA-48

6.3.4. In vitro dissolution study release study:

The BXR release pattern for drug loaded NPs was achieved in different simulated and biorelevant media. The rate of drug release from MCM-41 was appreciably higher with respect to plain BXR and BXR-NH_2-41. Release of BXR from BXR-41 was 3.33 times higher as compared to drug release from plain BXR in SIF media supplemented with enzyme pancreatin (pH 6.8). The BXR-41 took 75 min for the complete release of BXR in its competitive media *i.e.* SIF. Whereas the release was hindered for BXR-NH_2-41 due to the presence of amine moiety over the MSNs surface. Although the dissolution rate still showed 2.3 times higher drug release from BXR-NH_2-41 with respect to that of plain BXR after 360 min. Thus the release was controlled by amine grafting on the surface for the longer period of time. The principle of

overall increment in dissolution rate could be attributed to mesoporous assembly along with the amorphous nature of BXR. The dissolution rate for all three *i.e.* plain BXR, BXR-41 and BXR-NH_2-41 were slower in acetate media (pH 4.6) and SGF (pH 1.8) dissolution media enriched with pepsin enzyme. Although the release of drug filled bare and amine capped mesoporous assembly was still higher in this non-compatible media. Besides this, the dissolution profile was also conducted in enzyme free media also in order to check existence of interaction between the gelatin capsule shell and amine group of the aminated mesoporous nanotubes in the presence of enzyme. The result exhibited identical release in enzyme supplemented and enzyme lack SGF and SIF media as could be visualized from the figure 6.29. This strongly used as an evidence suggesting absence of interaction between gelatin shell and an amine group of the NPs. Furthermore, the release profile was also conducted in the fed state as well as in the fasted state gastric and intestinal media in order to figure out the influence of food on the *in vitro* dissolution rate. The result demonstrated considerable deviation of release pattern of FaSSGF from FeSSGF. Similar divergent results were obtained for FaSSIF and FeSSIF. The figure 6.29 displayed an incomplete release from BXR-41 and BXR-NH_2-41 in FaSSGF and FeSSGF. Although the result exhibited higher BXR release from both the aforesaid formulation in FeSSGF media in contrast to FaSSGF. On the flip side, they gave an almost complete release in FeSSIF media. The BXR release took about 75 min for the complete release (about 99%) from BXR-41 and 75% release after 360 min for FeSSIF for BXR-NH_2-41, whereas it was 58% and 31% after 360 min respectively in FaSSIF. This observation strongly inferred that BXR release is significantly affected by presence food. Thus, it could be anticipated that food could have a critical role in absorption as well in dissolution of BXR from its formulation.

Another formulation, *i.e.* BXR-48 exhibited superior release profile in contrast to BXR-41 where in the later formation required about 75 min for having a significant BXR release, whereas the former exhibited perhaps 45 min to complete emptying of BXR from its formulation named BXR-48 in pancreatin augmented SIF media (pH 6.8). This notable difference could be attributed to 3D cubic channel of MCM-48 which could perhaps contribute to burst BXR release for a shorter period of time. The dissolution rate was quite slow for BXR-NH_2-48 with respect to BXR-48 but it was superior with respect to BXR-NH_2-41. Moreover, the release was 5 times and 3.12 times higher with respect to release from pure BXR after 360 from BXR-48 and BXR-NH_2-48 respectively in SIF media.

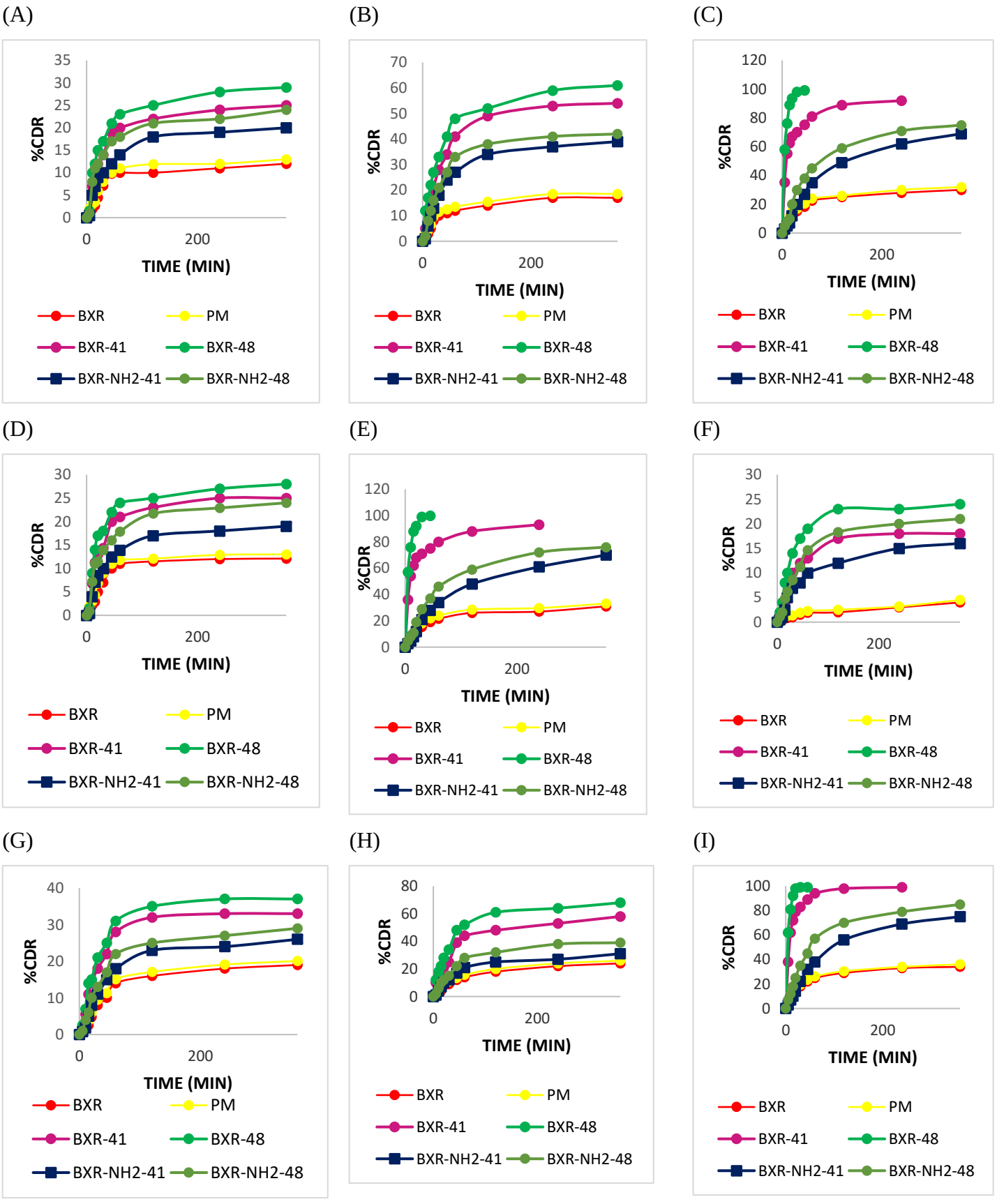

Figure 6.29: Dissolution rate profile of NPs in (A) SGF, (B) Acetate, (C) SIF, (D) FaSSGF, (E) FeSSGF, (F) FaSSIF, (G) FaSSIF

Further, the release pattern from fed and fasted state dissolution media exhibited identical results as encountered for MCM-41 NPs. Concisely, the release was higher for FeSSIF in contrast to FaSSIF, where drug release was completed within 45 min in the former media for BXR-48 and it took almost 6 h for 85% BXR release from BXR-NH_2-48. Whereas, only 68% and 39% of release was achieved after 360 min for BXR-48 and BXR-NH_2-48 in FaSSIF. This again puts the weightage of having a higher release in the presence of food. Overall, the dissolution release study suggested superior results for 3D cubic geometry as compared to 2D hexagonal assembly. Thus, it could be stated that MCM-48 NPs are best suited for solubility enhancement of BXR which is attributed to their unique 3D cubic structure. Furthermore, the release pattern of BXR from a physical mixture was comparable to plain BXR. This observation strongly suggests that encapsulation of drug inside the mesopores play a vital role on its release pattern.

6.3.5. In vitro diffusion study release study:

In vitro study was carried out in PBS solution at three different pH *viz.*, at 5.6, 6.8 and 7.4 representing release behaviour of BXR loaded MSNs in varied pH. Figure 6.30 depicts the release pattern of plain BXR, BXR-41, BXR-NH_2-41 and BXR-HA-41 in PBS solution. Results demonstrated rapid release of BXR at acidic pH (pH 5.6) from BXR-HA-41. In contrast, release of BXR was very slow at pH 7.4. A comprehensive pH responsive study demonstrated 18.5±0.11%, 83.5±0.98%, 64.87±1.38% and 92.17±0.57% cumulative BXR release from plain BXR, BXR-41, BXR-NH_2-41 and BXR-HA-41 in PBS 5.6 pH. Furthermore, it was 17%±1.56, 82.5±0.97%, 62.1±0.85 and 44.8±0.72% at pH 6.8 and 18.2±0.82%, 82.14±0.78%, 55.86±0.74% and 44.5±0.21% at pH 7.4 respectively for BXR, BXR-41, BXR-NH_2-41 and BXR-HA-41.

Figure 6.31 depicts the release pattern of plain BXR, BXR-48, BXR-NH_2-48 and BXR-HA-48 in PBS solution. Results demonstrated rapid release of BXR at acidic pH (pH 5.6) from BXR-HA-41. In contrast, release of BXR was very slow at pH 7.4. A comprehensive pH responsive study demonstrated 18.5±0.11%, 88.7±1.55%, 71.5±1.48% and 98.66±0.88% cumulative BXR release from plain BXR, BXR-41, BXR-NH_2-41 and BXR-HA-41 in PBS 5.6 pH. Furthermore, it was 17%±1.56, 86.2±1.77%, 67.1±0.15 and 49.7±0.82% at pH 6.8 and 18.2±0.82%, 87.14±0.99%, 59.7±0.34% and 48.5±0.71% at pH 7.4 respectively for BXR, BXR-48, BXR-NH_2-48 and BXR-HA-48.

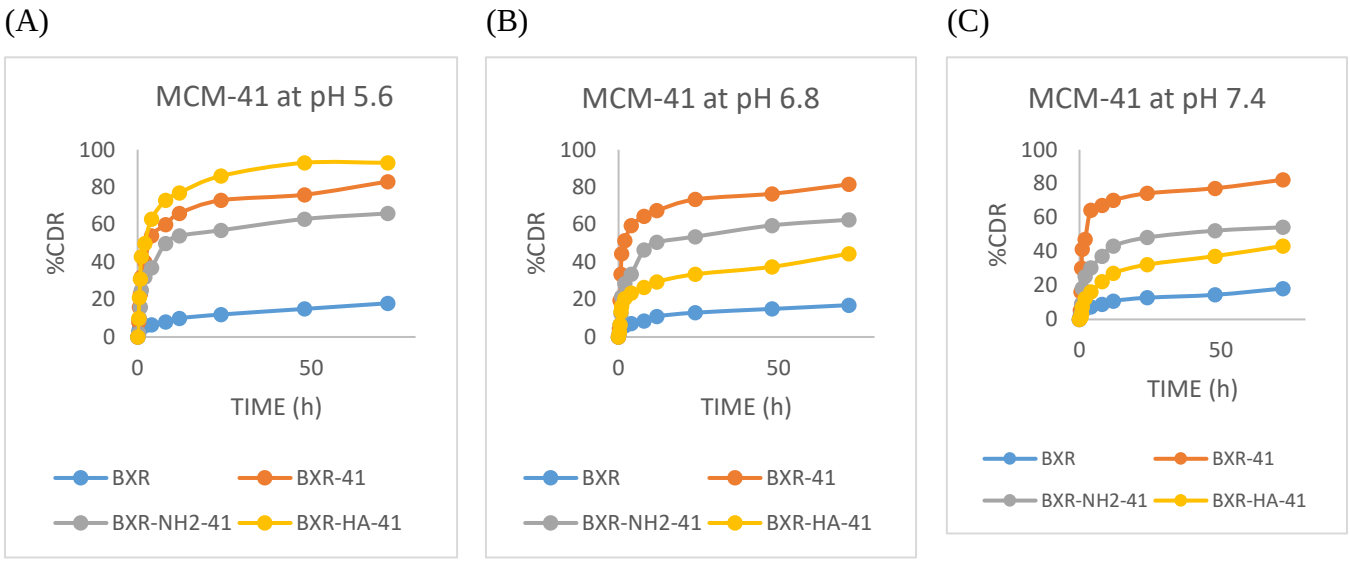

Figure 6.30: *In vitro* diffusion study of BXR encapsulated in MCM-41 in PBS solution at (A) pH: 5.6, (B) pH 6.8 and (C) pH 7.4

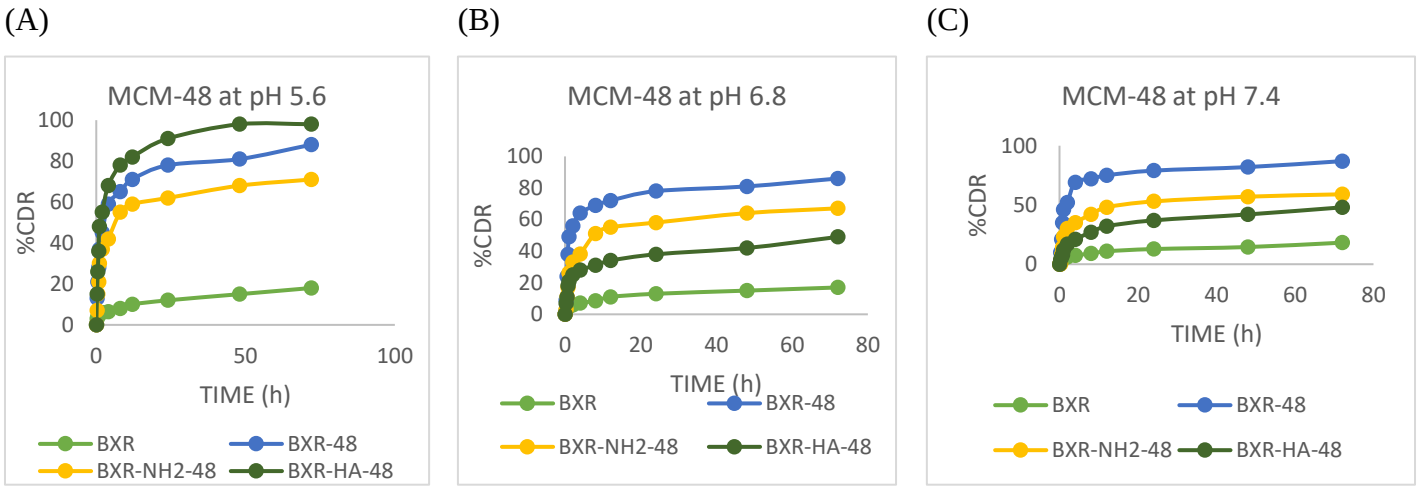

Figure 6.31: *In vitro* diffusion study of BXR encapsulated in MCM-48 in PBS solution at (A) pH: 5.6, (B) pH 6.8 and (C) pH 7.4

6.3.6. In vitro cytotoxicity study on Caco-2 cell line for oral formulation:

MTT assay was performed to screen out the maximum concentration of BXR loaded nanoparticle up to which they could be utilized to carry out the *in vitro* permeability study. Herein, the MTT assay was performed for drug free nanoparticles and drug loaded nanoparticles on the received Caco-2 cell line incubating for 4 h. The result demonstrated the safe nature of plain and BXR loaded nanoparticles toward Caco-2 cells in the concentration range of 10-100 µM. The %relative viability was >98.57±0.71% for drug free bare and amine coated nanoparticles (figure 6.32A). Whereas the %relative viability was >95.20±0.74% for BXR-41, BXR-48, BXR-NH_2-41 and BXR-NH_2-48 as shown in figure 6.32B.

(A)

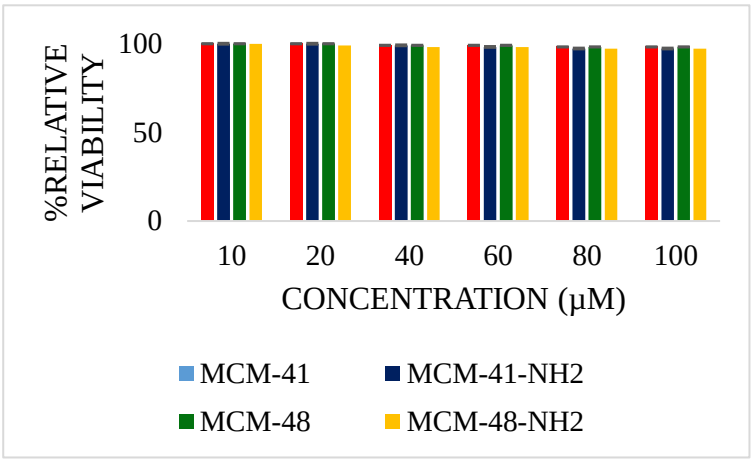

(B)

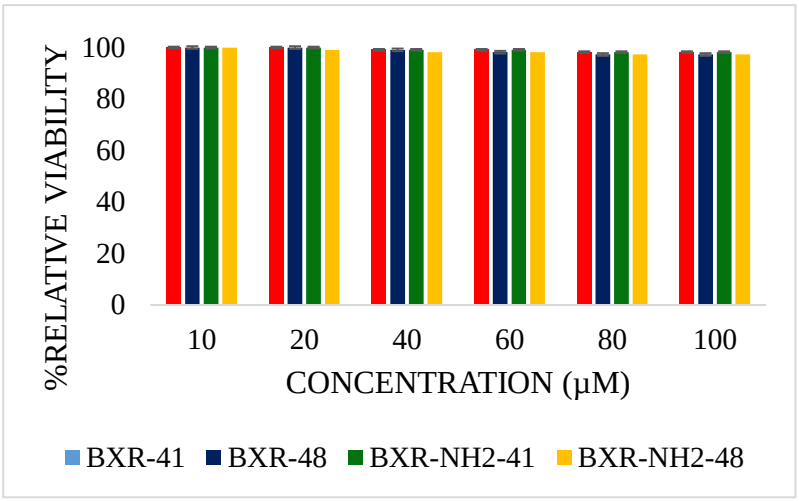

Figure 6.32: Cell viability graph for (A) drug free and (B) drug filled bare and amine coated nanoparticles

6.3.7. In vitro cytotoxicity study on MCF-7 cell line for parenteral formulation:

The concentration and time dependent cell cytotoxicity study in the range of 0.1-100 µM concertation for 24 and 72 h respectively was performed for MCM-41, MCM-NH_2-41, MCM-HA-41 and MCM-48, MCM-NH_2-48, MCM-HA-48. The investigation outcome revealed 99.20 ± 0.75, 97.20 ± 0.71 and 96.87 ± 0.72 %relative viability for MCM-41, MCM-NH_2-41 and MCM-HA-41 respectively for 24 h. Further the values for the same were >95% even after 72 h also. Similarly, the results for MCM-48, MCM-NH_2-48 and MCM-HA-48 demonstrated %relative viability above 96% for engineered formulation after 24 and 72h (figure 6.33).

(A)

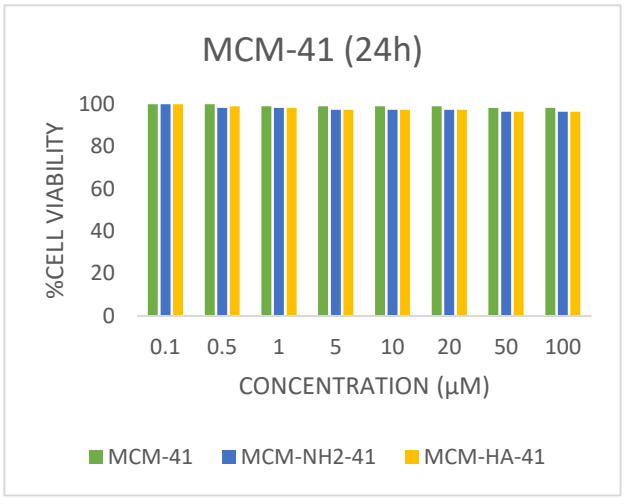

(B)

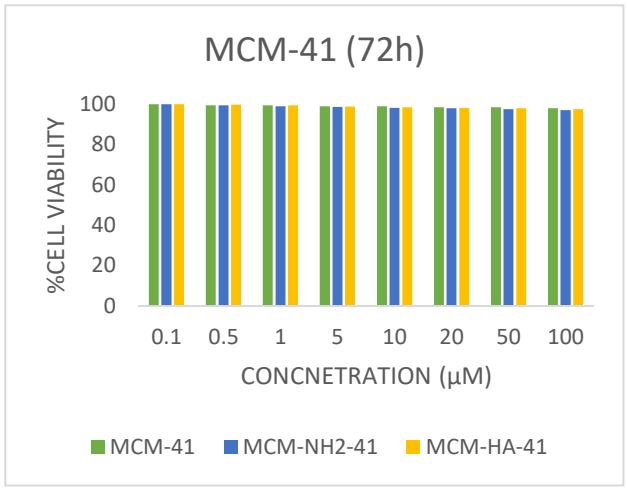

(C)

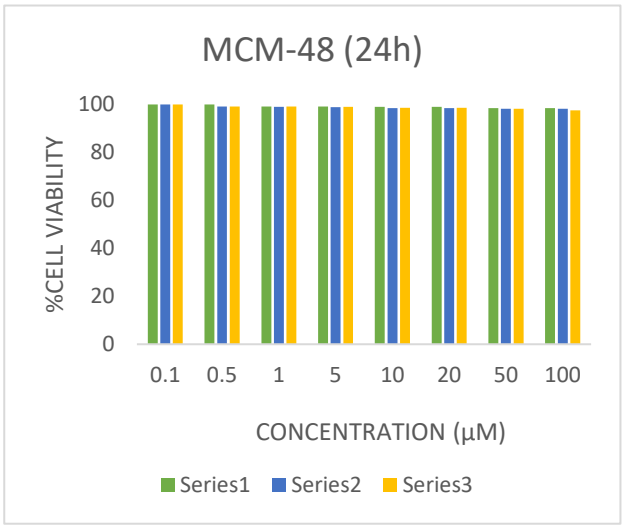

(D)

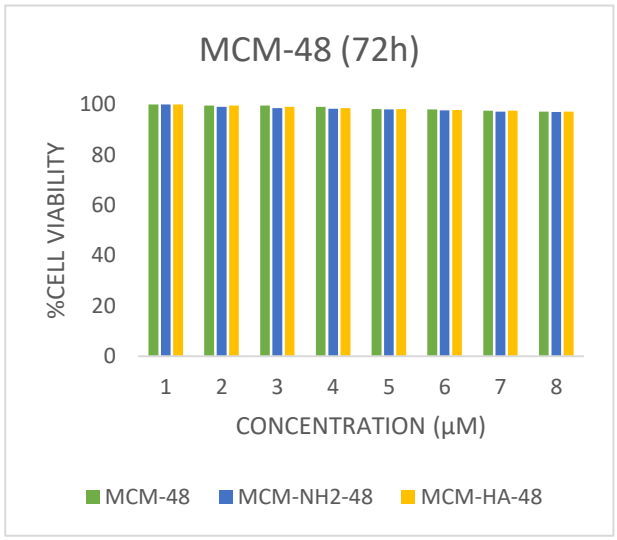

Figure 6.33: Cell viability graph for drug free MCM-41 type of nanoparticles after (A) 24h and (B) 72h; and for MCM-48 type of nanoparticles after (C) 24h and (D) 72h

Besides this the similar study was also carried out for BXR, BXR-41, BXR-NH_2-41, BXR-HA-41 and BXR-48, BXR-NH_2-48, BXR-HA-48 in the range of 1-8 µM concertation for 24 and 72 h respectively. The result showed 75.89 ± 1.08, 45.98 ± 0.87, 67.28±0.12 and 38.98±0.77 %relative viability and 70.82 ±0.28, 40.25 ± 0.95, 62.55±0.98 and 19.07±0.14 %relative viability after an incubation time of 24h and72 h respectively for MCM-41 type of carriers. Whereas the result was showing 75.89 ± 1.08, 42.45 ± 0.86, 64.58±0.94 and 35.97±0.79 %relative viability and 70.82 ± 1.38, 36.44± 0.75, 58.91±0.52 and 15.47±0.87 %relative viability for BXR-48, BXR-NH_2-48 and BXR-HA-48 after 24h and 72h respectively (figure 6.34). Thus, it could be stated that the degree of cytotoxicity is purely attributed to drug

moiety encapsulated in the MSNs. Further the IC50 obtained for each formulation is mentioned in below table 6.7 and table 6.8.

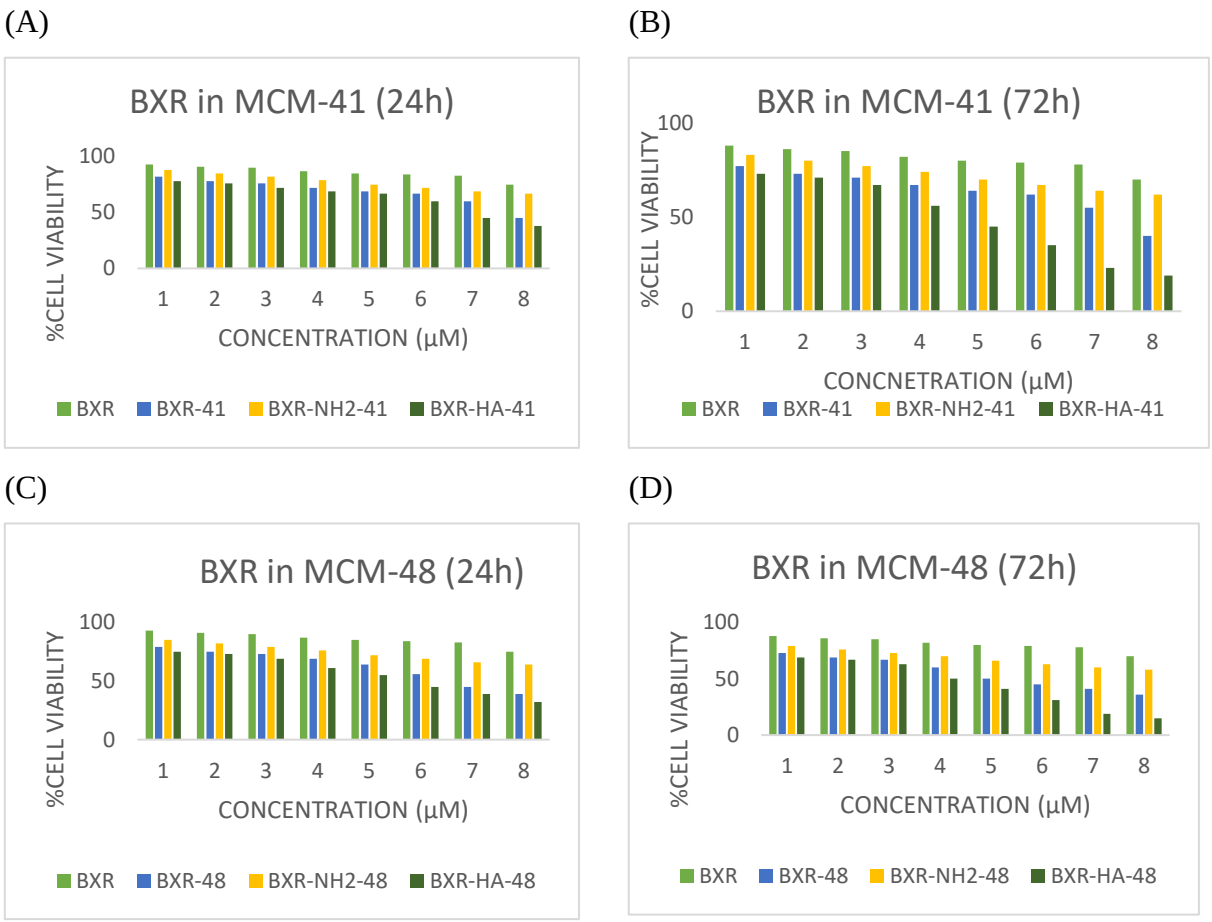

Figure 6.34: Cell viability graph for drug loaded MCM-41 type of nanoparticles after (A) 24h and (B) 72h; and for MCM-48 type of nanoparticles after (C) 24h and (D) 72h

Table 6.7: IC_{50} values for BXR nanoparticles encapsulated in MCM-41

Time (h)	Concentration with respect to IC_{50} (µM)*			
	BXR	BXR-41	BXR-NH_2-41	BXR-HA-41
24	>8	7.87±0.38	>8	6.83±0.51
72	>8	6.59±0.51	>8	4.27±0.89

* The study was conducted in three replicates and results were displayed in mean±S.D.

Table 6.8: IC_{50} values for BXR nanoparticles encapsulated in MCM-48

Time (h)	Concentration with respect to IC_{50} (µM)*			
	BXR	BXR-48	BXR-NH_2-48	BXR-HA-48
24	>8	6.51±0.489	>8	5.54±0.17
72	>8	5.12±0.71	>8	3.99±0.52

* The study was conducted in three replicates and results were displayed in mean±S.D.

6.3.8. In vitro permeability study for oral formulation:

From the MTT cytotoxicity study BXR concentration was selected to be 100 µg/mL concentration was considered to be a safe concentration as it was having no negative influence on the Caco-2 cell viability. A Transport experiment was performed for BXR release evaluation from apical to basal compartment transportation. Wherein, the P_{app} value was estimated at the end of 24 h calculated individually for different formulation as listed in the table 6.9. The data revealed nearly 3.79 and 4.66-fold increment in the permeability for BXR-41 and BXR-48 respectively, whereas the coefficient value was declined for BXR-NH_2-41 and BXR-NH_2-41 with respect to bare nanoparticle but these were still greater as compared to permeability of pure BXR *i.e.* 2.28 and 2.71 respectively. Therefore, the permeability results unveiled enhanced permeability of BXR by designing and encapsulating them into mesoporous nanosystem.

Table 6.9. Permeability study of formulated nanoparticles

TIME (min)	BXR	BXR-41	BXR-48	BXR-NH_2-41	BXR-NH_2-48
30	0.65±0.04	4.39±0.55	4.96±0.72	2.45±0.46	3.56±0.51
60	1.52±0.22	11.87±1.22	15.67±1.26	6.39±1.27	9.93±1.38
90	3.81±0.56	21.17±1.64	25.49±1.89	9.47±1.54	13.32±1.66
120	5.93±0.87	26.53±1.87	32.88±2.04	13.89±1.85	19.57±2.17
180	6.99±1.07	32.08±2.56	38.15±2.98	21.06±2.08	25.24±2.56
240	9.82±1.39	38.94±2.77	43.07±3.01	25.44±2.34	30.08±2.82
300	11.12±1.84	42.65±3.35	49.83±3.47	29.58±2.67	31.82±3.05
dQ/dt	0.037±0.055	0.14±0.12	0.17±0.42	0.09±0.04	0.10±0.07
P_{app}	$1.96*10^{-2}$	$7.43*10^{-2}$	$9.14*10^{-2}$	$4.47*10^{-2}$	$5.31*10^{-2}$

6.3.9. Cellular uptake by confocal microscopy:

The FITC labelled MSNs were visualized under confocal microscope. The images demonstrated a relatively higher uptake of MCM-HA-41 with respect to HA+MCM-HA-41 after 24h. Figure 6.35 demonstrated a blue coloured nucleus after staining with DAPI. When the MCF-7 cells are incubated with the FITC labelled HA coated nanoparticles, it showed a strong green fluorescence surrounding the nuclei, indicates a successful internalization of HA coated nanoparticles. Whereas the FITC labelled pristine nanoparticle showed weaker fluorescence with respect to surface coated nanoparticles. This outcome states the relatively

lower efficiency of uncoated nanoparticle for the target side. The similar results were obtained for MCM-48 types of nanoparticles (figure 6.36).

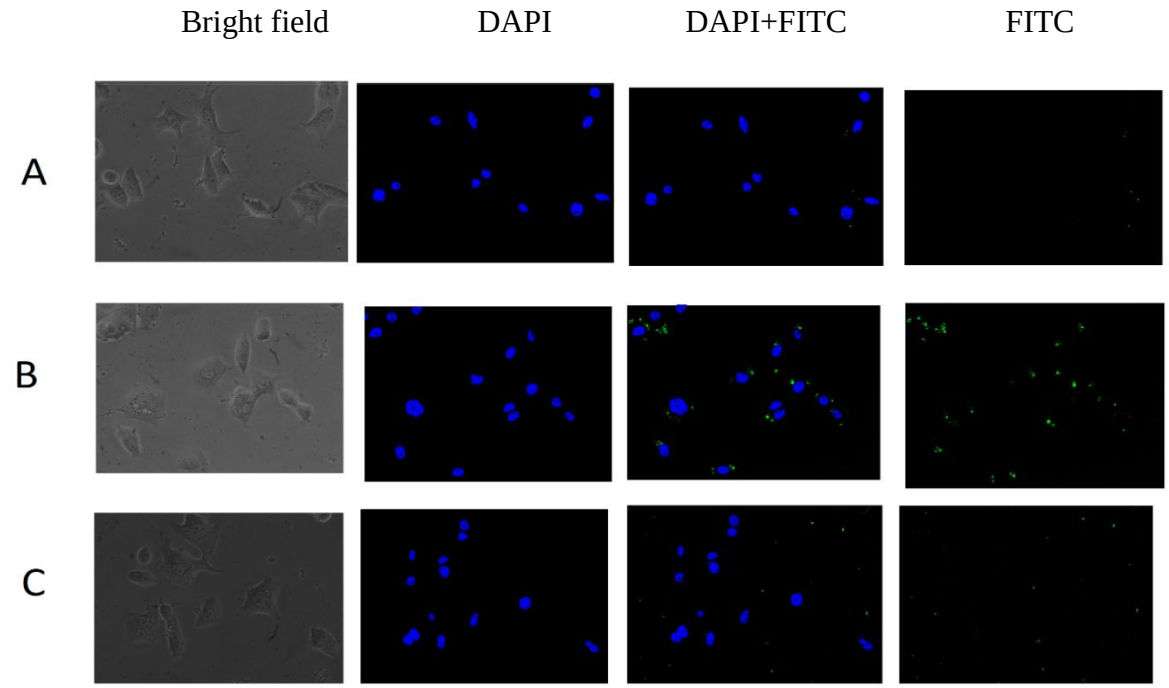

Figure 6.35. Confocal microscopic images of cellular uptake of FITC labelled MSNs (green) in MCF-7 cell line with DAPI nuclear staining(blue) for (A) MCM-NH_2-41, (B) MCM-HA-41, and (C) HA+ MCM-HA-41

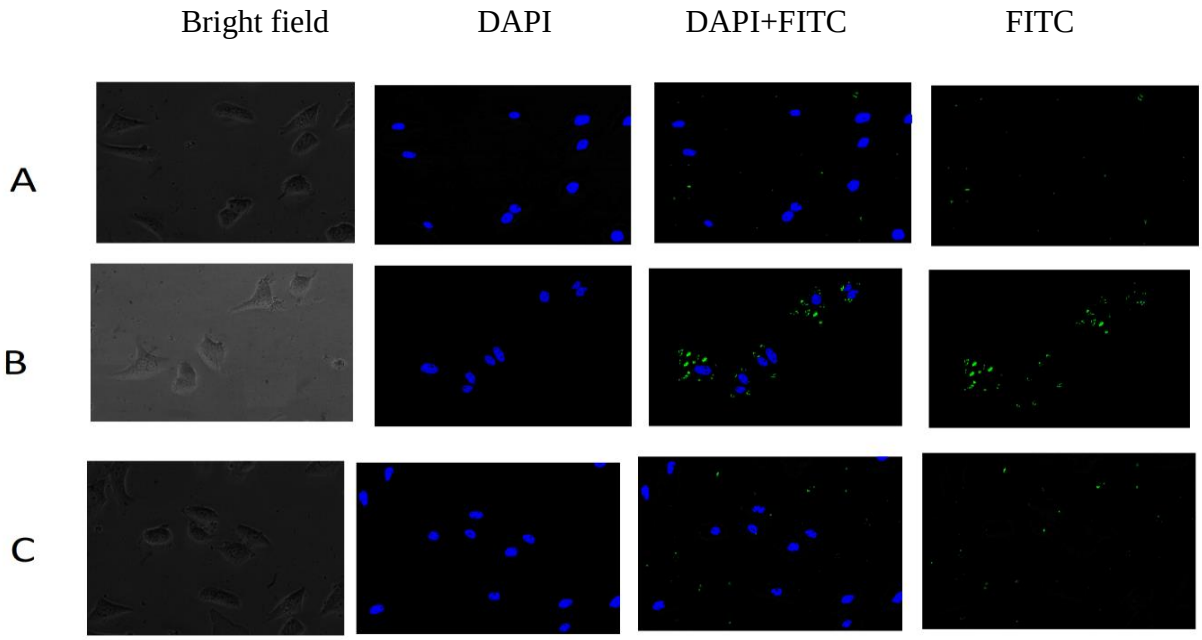

Figure 6.36. Confocal microscopic images of cellular uptake of FITC labelled MSNs (green) in MCF-7 cell line with DAPI nuclear staining(blue) for (A) MCM-NH_2-48, (B) MCM-HA-48, and (C) HA+ MCM-HA-48

6.3.10. Cellular uptake by FACS

To provide a quantitative comparison, the cellular uptake performance of aminated and surface coated nanoparticles in MCF-7 was further studied by FACS analysis. After treating MCF-7 cells with FITC labelled HA-MSNs for 24h, the FITC signal emitted from the cells were very strong (Fig. 6.37 and 6.38), indicating a high cellular uptake of HA-MSNs. In contrast, the mean intensity of FITC from the cells incubated with FITC labelled MSNs without surface modification is only 19.57% and 21.89% respectively for MCM-NH_2-41 and MCM-NH_2-48. Moreover, FITC labelled MCM-HA-41 and MCM-HA-48 showed 82.91% and 85.88% uptake by MCF-7 cells respectively. To further confirm the specific interaction of HA-MSNs with MCF-7 cells, free HA (10 mg/mL) was added prior to the addition of FITC labelled HA-MSNs in the cell culture medium. The FITC signal intensity decreases by 38% and 42% compared to the FITC labelled MCM-HA-41 and MCM-HA-48 respectively, suggesting that the interaction between free HA and HA-MSNs and the subsequent CD44 receptor-mediated endocytosis has been weakened due to the competition of free HA. The above results have confirmed that HA-MSNs can target CD44 over-expressing MCF-7 cancer cells via the CD44 receptor-mediated endocytosis pathway and show an improved endocytosis performance compared to the unmodified MSNs. The FACS results provide a quantitative comparison, which is consistent with the confocal microscopy observations (Fig. 6.37 and 6.38A-C).

(I) (II) (III)

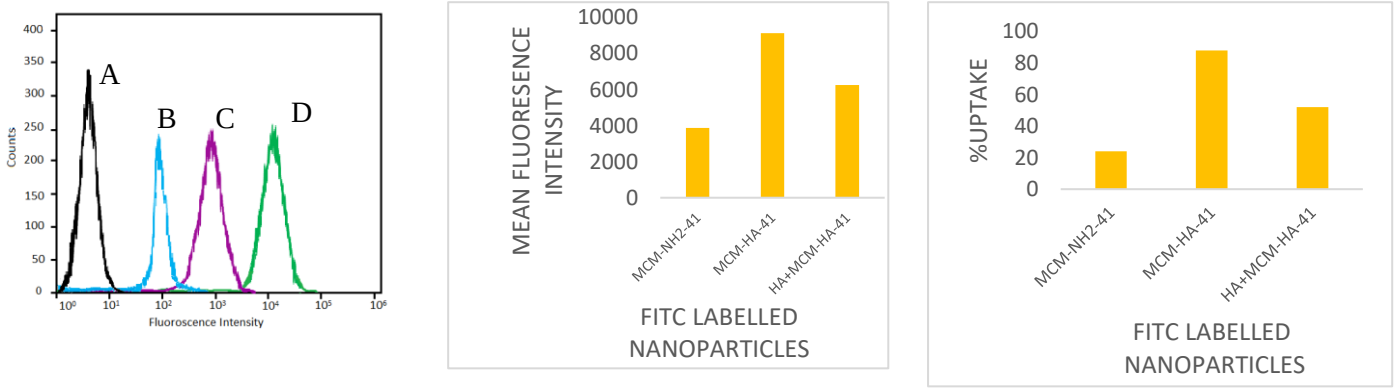

Figure 6.37: (I) Flow cytometric (II) mean fluorescence intensity and (III) %uptake data for synthesized nanoparticles

*(A) untreated cells (control), (B) MCM-NH_2-41, (C) HA+MCM-HA-41, (D) MCM-HA-41

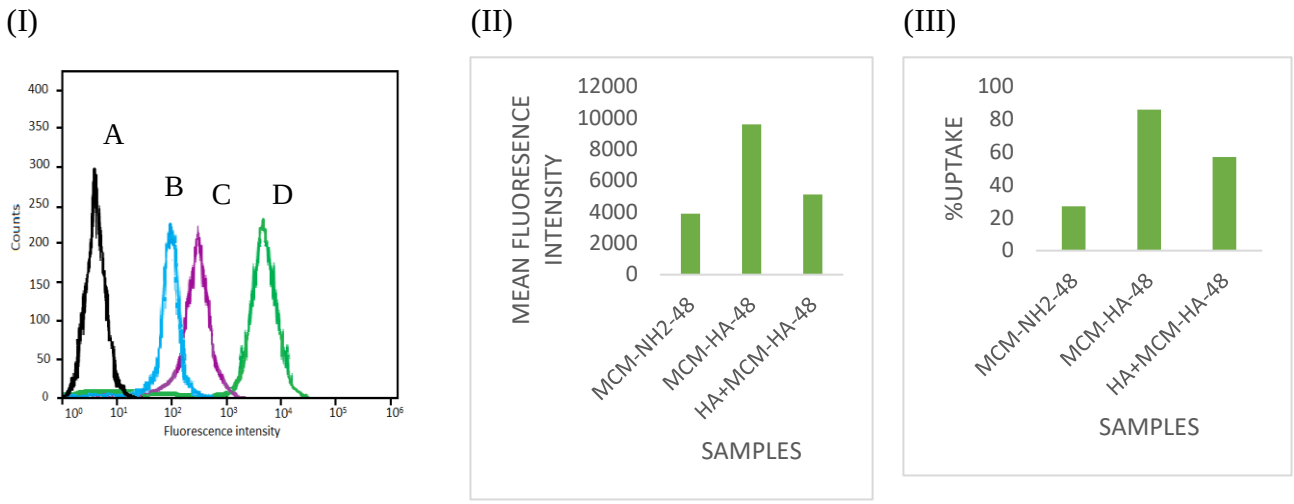

Figure 6.38: (I) Flow cytometric (II) mean fluorescence intensity and (III) %uptake data for synthesized nanoparticles

*(A) untreated cells (control), (B) MCM-NH_2-41, (C) HA+MCM-HA-41, (D) MCM-HA-41

6.3.11. Apoptosis assay:

The death mechanisms were adjudged by FACS protocol using Annexin V-FITC apoptosis detection kit. The cells were treated with BXR, BXR-NH_2-41and BXR-HA-41. For MCF-7 cells, early apoptosis was observed as 4.98%, 11.77% and 59.27% in cells treated with BXR, BXR-NH_2-41 and BXR-HA-41. respectively. BXR could induce very less early apoptosis in the cells due to poor internalization into cells. Notably, drug loaded nanoparticles led to early and late apoptosis induction in within 24 h in MCF-7 cells. Remarkably BXR-HA-41 were capable of inducing higher early and late apoptotic cells percentage than BXR-NH_2-41. It can be concluded that target group played a major role in giving this outcome. A similar pattern was observed for MCM-48 types of nanoparticles as well alongwith 6.17%, 15.44% and 63.21% early apoptosis. (figure 6.39).

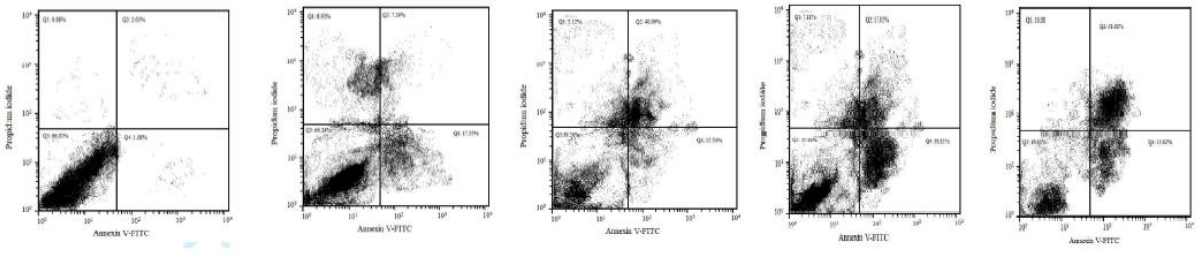

Figure 6.39: apoptosis study for (A) BXR, (B) BXR-NH_2-41, (C) BXR-NH_2-48, (D) BXR-HA-41 and (E) BXR-HA-48

6.3.12. Haemolysis study:

Detailed investigation of heamolysis analysis demonstrated safe nature of formulated nanoparticles. The microscopic analysis for the same is depicted in the figure 6.40. The microscopic image for the RBC treated with Triton X-100 and plain BXR showed ruptured and deformed erythrocytes. Whereas the integrity remained unchanged after treating the RBCs with nanoparticles. Furthermore, the spectral analysis demonstrated 1.86 ± 0.72 and 1.35 ± 0.53% % heamolysis for BXR-HA-41 and BXR-HA-48 respectively whereas the value was higher than 5% in case of pure BXR.

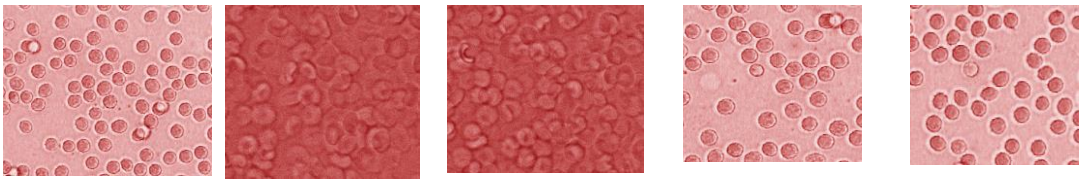

(A) (B) (C) (D) (E)

Figure 6.40. Microscopical and visual images for (A) negative control (B) positive control (C) BXR, (D) BXR-HA-41 and (E) BXR-HA-48

6.3.13. In vivo pharmacokinetics study for oral formulation:

Poor bioavailability of the BXR is due to limited solubility in water and its extensive first pass metabolism. *In vivo* bioavailability of free BXR and BXR loaded nanoparticles was studied in Swiss albino female mice. Following the sample preparation protocol as mentioned in the earlier section the plasma samples were comprehensively analyzed by optimized and validated RP-HPLC method. Different pharmacokinetic parameters for plain BXR, BXR-41, BXR-48, BXR-NH_2-41 and BXR-NH_2-48 were compared with each other and summarized in the following table 6.10. The pharmacokinetic study outcome revealed significant increment in drug plasma concentration ($p<0.05$) on the administration of formulated nanoparticle in contrast to plain drug. Furthermore, the comparison in the C_{max} value for BXR-41 and BXR-48 divulged higher value of C_{max} for latter nanoparticles. The considerable high plasma concentration after oral administration of BXR-41 and BXR-48 was achieved in 60 min with 12.58 and 13.65 plasma concentration compared to 4.12 C_{max} value after 1 h for plain BXR. The maximum concentration obtained within 60 min followed by steady fall, which is an indication of the lag period continuing up to 300 min. The result gathered here were complementary to the *in vitro* release data wherein the higher BXR release was obtained from BXR-48. Moreover, the lesser C_{max} figure for aminated nanoparticle with respect to bare nanoparticle could be attributed to hindered BXR release due to the presence of an amine group

over the surface. But, the results were still favoring the aminated nanoparticles over plain BXR. Similarly, the $AUC_{(0-24)}$ and $AUC_{(0-infinite)}$ results demonstrated identical pattern of increment as observed for C_{max}. Thus an overall increment in the bioavailability were 3.05, 3.31, 2.06 and 2.21 fold for BXR-41, BXR-48, BXR-NH_2-41 and BXR-NH_2-48 respectively with respect to the BXR pure drug as listed in table 6.10. The significant increase in AUC for BXR nanoparticle could be due the nano size of the formulation and avoidance of the first pass metabolism through the lymphatic transport pathway. The increment in the bioabailability could be attributed to enhanced solubility of BXR in the gastrointestinal tract encapsulating them into MSN framework (figure 6.41).

Table 6.10: Pharmacokinetics parameters for BXR, BXR-41, BXR-48, BXR-NH_2-41 and BXR-NH_2-48

PARAMETERS	BXR	BXR-41	BXR-48	BXR-NH_2-41	BXR-NH_2-48
C_{max} (µg/ml)	4.12 ±0.19	12.58±0.24	13.65±0.35	8.51±0.11	9.12±0.16
$AUC_{(0-24)}$ (µg/ml*h)	14.24 ±0.04	43.68±0.25	50.34±0.44	91.64 ±0.04	97.24±0.08
$AUC_{(0-infinite)}$ (µg/ml*h)	16.55±0.17	45.89±0.32	53.51±0.23	130.82 ±0.18	134.12±0.14
$T_{1/2\ (h)}$	3.28 ±0.06	6.12±0.26	6.45±0.12	11.47 ±0.05	12.91±0.11
MRT (h)	3.39±0.58	7.14±0.55	7.47±0.44	17.25±0.58	18.30±0.47
CL(mg)/(µg/ml)/h	0.89±0.45	0.32±0.09	0.28±0.07	0.13±0.84	0.11±0.58
Relative bioavailability	-	3.05	3.31	2.06	2.21

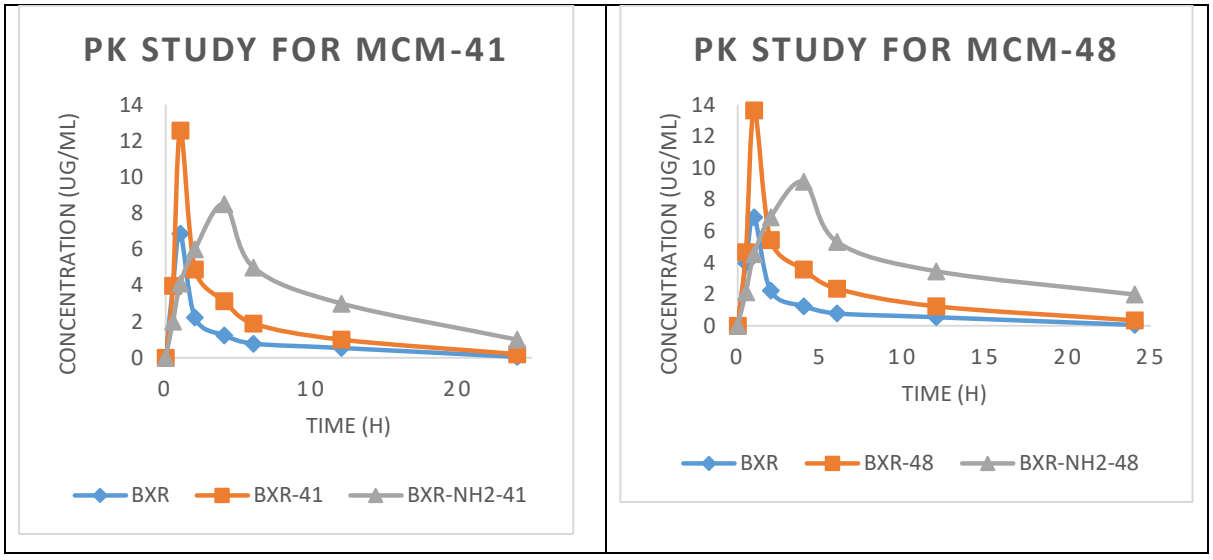

Figure 6.41: *In vivo* pharmacokinetics study for MCM-41 and MCM-48 type of nanoparticles

6.3.14 In vivo pharmacokinetics and biodistribution study for parenteral formulation:

Statistically significant differences were found in the major pharmacokinetic parameters between BXR and formulations. Free BXR exhibited a more rapid clearance from blood with low $t_{1/2}$ and peak plasma concentration. Whereas, HA coated nanoparticles exhibited a slow and steady clearance with longer $t_{1/2}$ and higher AUC, where higher $t_{1/2}$ indicates the ability of nanocarriers to accumulate at tumour site for a longer time and give enhanced therapeutic effect. The details of pharmacokinetic parameters is summarized in table 6.11 and it is depicted in the figure 6.42

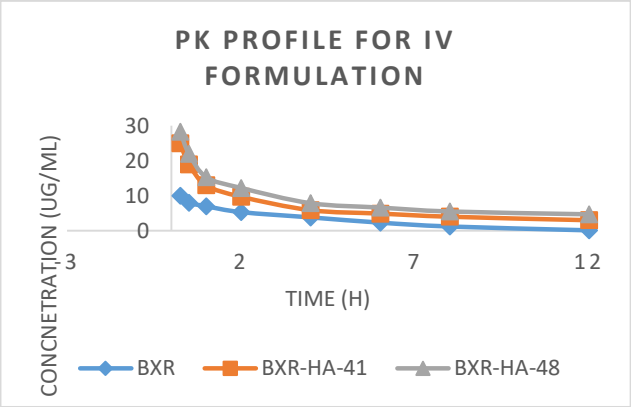

Figure 6.42: *In vivo* pharmacokinetics study for (A) BXR, (B) BXR-HA-41 and (C) BXR-HA-48

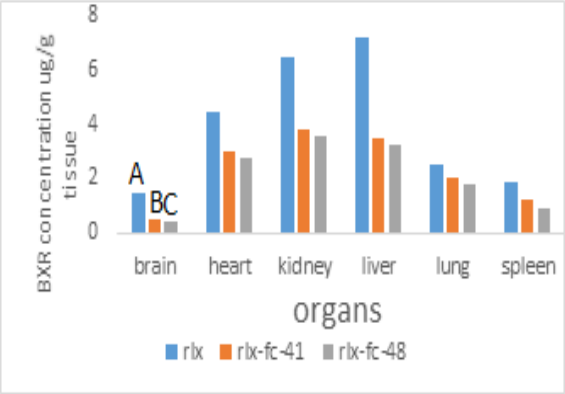

Figure 6.43: Biodistribution graph for (A) BXR, (B) BXR-HA-41 and (C) BXR-HA-48 in different organs

Table 6.11: Pharmacokinetics parameters for BXR, BXR-HA-41 and BXR-HA-48

PARAMETERS	BXR	BXR-HA-41	BXR-HA-48
C_{max} (µg/ml)	9.8±0.6	25.67±0.5	28.34±0.1
$AUC_{(0-24)}$ (µg/ml*h)	41.52±01.2	99.41±1.97	104.61±1.47
$T_{1/2\ (h)}$	41.74±0.6	157.82±2.13	178.0±2.62
MRT (h)	2.83±0.07	10.43±0.9	13.87±1.1
Vss (mg)/(µg/ml)	0.51±0.04	0.55±0.03	0.58±0.05
Cl(mg)/(µg/ml)/h	0.17±0.09	0.07±0.01	0.04±0.01

The concentration of BXR in major organs was determined at 24 h. From results it could be inferred that concentration of BXR-HA-41 and BXR-HA-48 in all major organs were remarkably decreased as compared to BXR alone. Thus, the nanoparticle showed lesser accumulation in all major organs than free drug. This might be due to prolonged blood

circulation of MSNs in bloodstream thus reducing major side effects associated with BXR (figure 6.43).

Finally, the histological examination was performed to investigate safety profile of engineered formulations. The figure 6.44 shows the histological images for plain BXR and BXR loaded nanoparticles. The images revealed no histological evidence of any toxicity in the mice which were given BXR formulation. Thus, it could be concluded that the formulated nanoparticles are safe and not having any toxicity on the major organs.

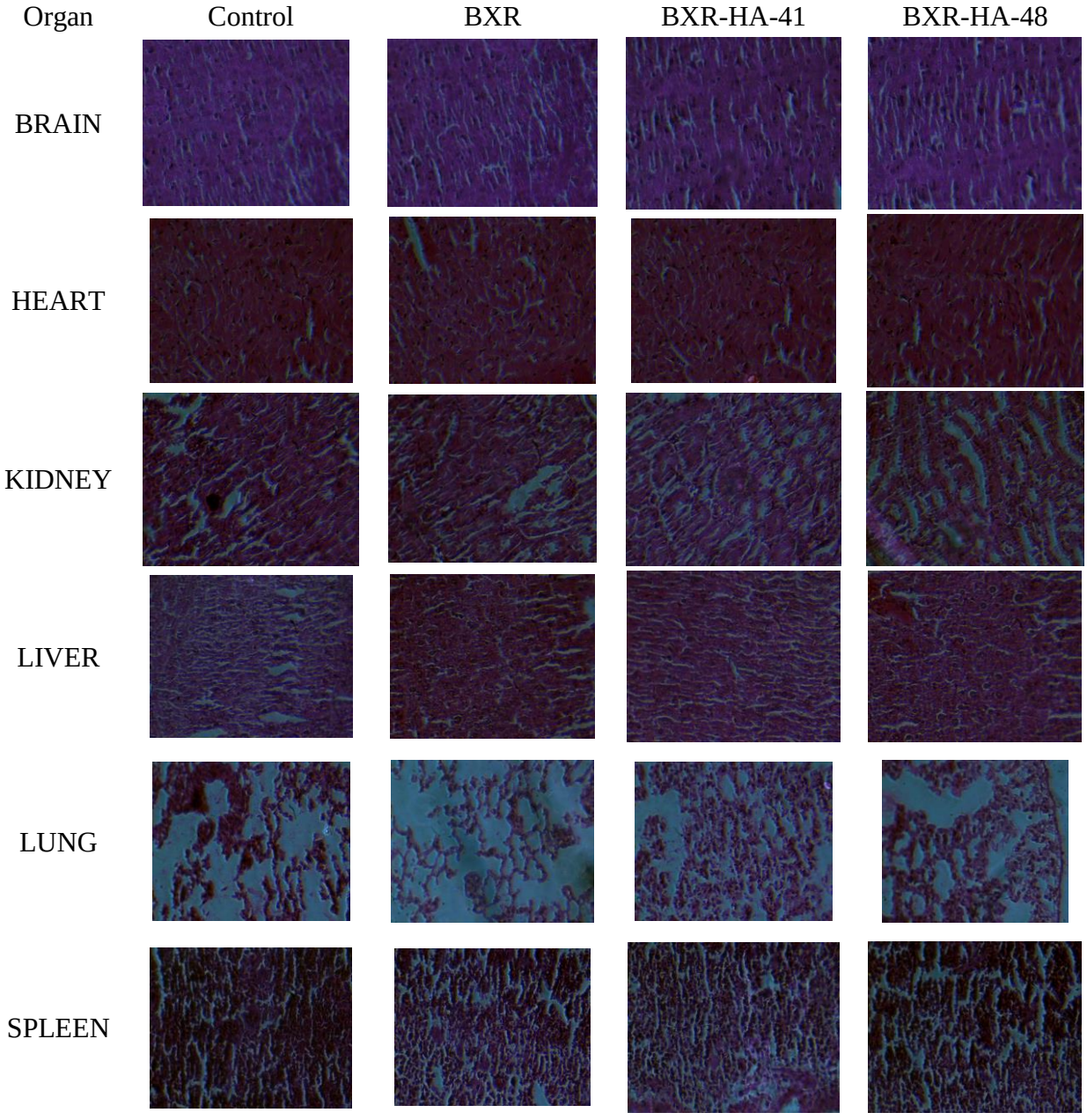

Figure 6.44: Histological images for different formulation given to mice

6.3.16. Stability study of synthesized nanoparticle:

The DSC and SXRD data revealed that the synthesized nanoparticles were stable at 40±2 ºC and 75±5 %RH for the 6 months. The instrumental data revealed identical DSC and SXRD pattern at 0^{th} day and after 6^{th} month as depicted in figure 6.45 and figure 6.46 which strongly supports no degradation or lack of unstability of formulated nanoparticles. In the DSC thermogram of nanoparticles, the peak of BXR was absent which strongly suggest that on storage there was no leakage of drug. Furthermore, identical SXRD pattern at 0^{th} month and after 6^{th} month revealed that the mesoporous skeleton were well preserved.

(A)

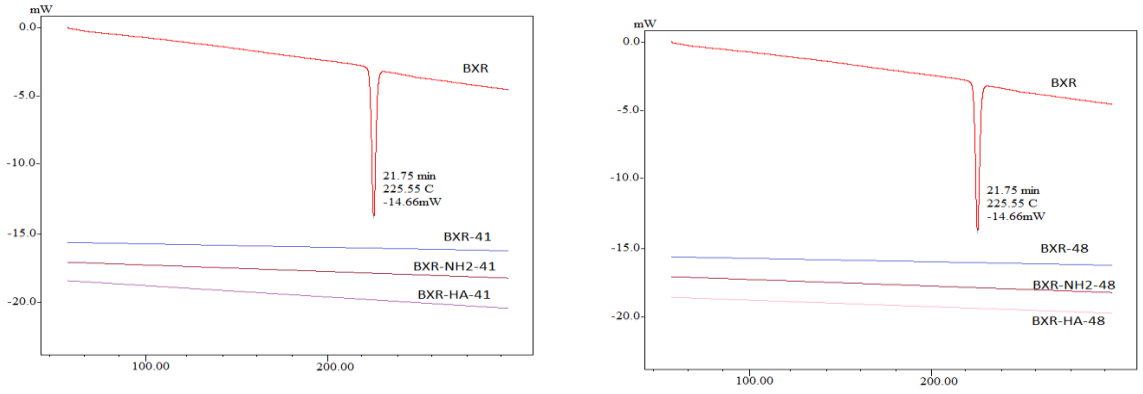

(B)

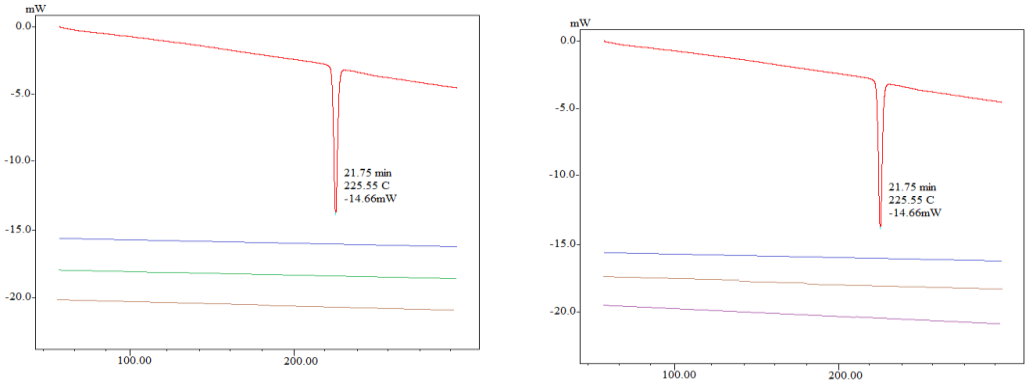

Figure 6.45: DSC thermogram of different nanoparticles at (A) 0^{th} month and (B) 6^{th} month

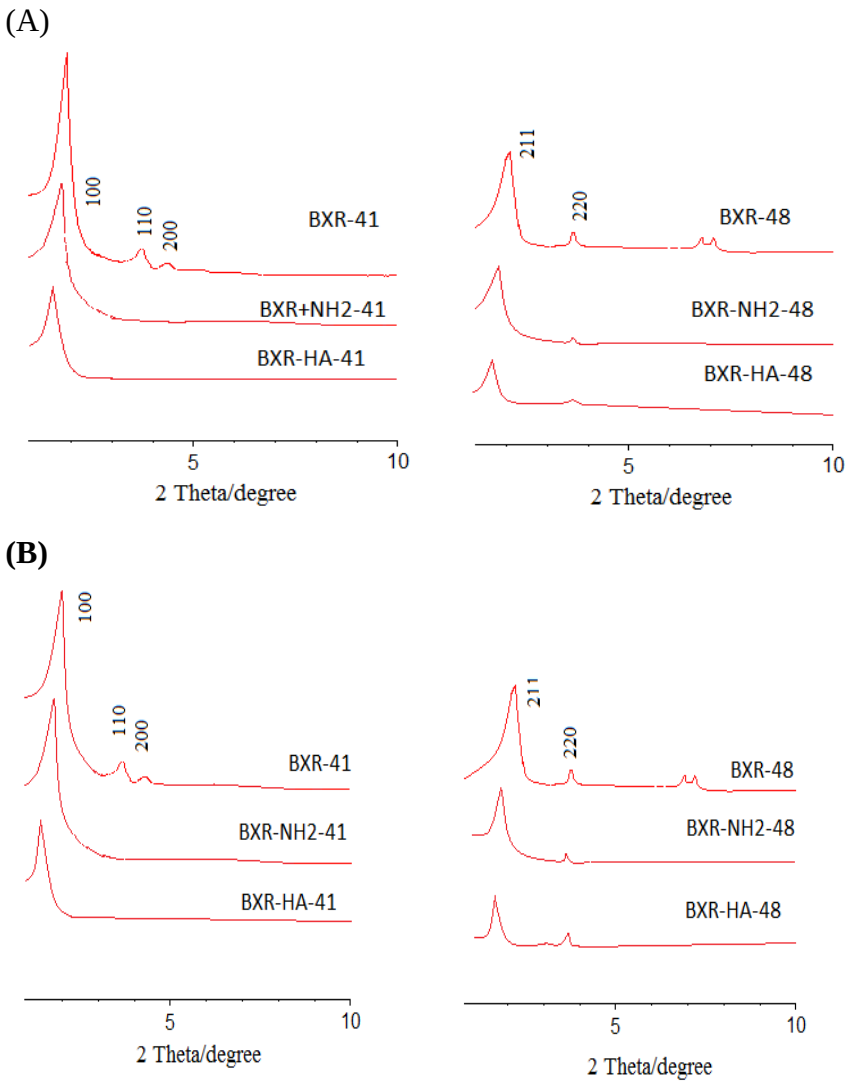

Figure 6.46: SXRD pattern of different nanoparticles at (A) 0th month and (B) 6th month

6.4. Conclusion:

Form the entire study it could be concluded that encapsulation of BXR inside the mesopores of MCM-41 and MCM-48 remarkably improved its drug release profile as well its permeability and thereby the bioavailability was also significantly enhanced. *In vitro* release data exhibited a burst BXR release having a magnitude of 3.3 and 5 times enhancement in the solubility by BXR-41 and BXR-48 with respect to BXR plain drug. In contrast, though the surface decorated nanoparticle exhibited incomplete BXR release after a period of 300 min, the release were still higher compare to API *i.e.* 2.3 and 3.12 times for BXR-NH_2-41 and BXR-NH_2-48 with respect to pure BXR

The *in vitro* permeability data revealed nearly 3.79 and 4.66 fold increment in the permeability for BXR-41 and BXR-48 respectively, whereas the permeability coefficient value was declined for BXR-NH_2-41 and BXR-NH_2-48 with respect to bare nanoparticle but these were still greater as compared to permeability of pure BXR *i.e.* 2.28 and 2.71 respectively. Therefore, the permeability results unveiled enhanced permeability of BXR by designing and encapsulating them into mesoporous nanosystem. The *in vivo* investigation revealed an overall 3.01, 3.31, 2.06 and 2.21 fold increment in the bioavailability with respect to the BXR pure drug. The increment in the bioabailability could be attributed to enhanced solubility of BXR in the gastrointestinal tract encapsulating them into MSN framework. Additionally, the cellular uptake study for HA coated nanoparticles evidenced higher uptake of surface functionalized nanoparticles compared to bare nanoparticles. This investigation unveiled 3.8 and 4.2 times increment in cellular uptake for MCM-HA-41 and MCM-HA-48 respectively as compared to pristine nanoparticles. This could be helpful in directing the drug release to cancer cells only and thereby also help in dose reduction as well as its adverse effect to healthy cells as the amount reaching to non-tumor cells would be decreased by surface coating. Lastly, the histological examination and biodistribution study demonstrated safe nature of engineered nanoaprticles.

6.5. References:

1. Qu L, Tang X. Bexarotene: a promising anticancer agent. Cancer chemotherapy and pharmacology. 2010;65(2):201-5.
2. Yang L, Tin-U C, Wu K, Brown P. Role of retinoid receptors in the prevention and treatment of breast cancer. Journal of mammary gland biology and neoplasia. 1999;4(4):377-88.
3. Chen L, Wang Y, Zhang J, Hao L, Guo H, Lou H, et al. Bexarotene nanocrystal—oral and parenteral formulation development, characterization and pharmacokinetic evaluation. European Journal of Pharmaceutics and Biopharmaceutics. 2014;87(1):160-9.
4. Wu K, Kim H-T, Rodriquez JL, Hilsenbeck SG, Mohsin SK, Xu X-C, et al. Suppression of mammary tumorigenesis in transgenic mice by the RXR-selective retinoid, LGD1069. Cancer Epidemiology and Prevention Biomarkers. 2002;11(5):467-74.
5. Chen C, Sun W, Wang X, Wang Y, Wang P. pH-responsive nanoreservoirs based on hyaluronic acid end-capped mesoporous silica nanoparticles for targeted drug delivery. International journal of biological macromolecules. 2018;111:1106-15.
6. Zhao Q, Geng H, Wang Y, Gao Y, Huang J, Wang Y, et al. Hyaluronic acid oligosaccharide modified redox-responsive mesoporous silica nanoparticles for targeted drug delivery. ACS applied materials & interfaces. 2014;6(22):20290-9.
7. Khushalani D, Kuperman A, Ozin GA, Tanaka K, Coombs N, Olken MM, et al. Metamorphic materials: restructuring siliceous mesoporous materials. Advanced materials. 1995;7(10):842-6.
8. Schumacher K, Grün M, Unger K. Novel synthesis of spherical MCM-48. Microporous and Mesoporous Materials. 1999;27(2):201-6.
9. Ebrahimi-Gatkash M, Younesi H, Shahbazi A, Heidari A. Amino-functionalized mesoporous MCM-41 silica as an efficient adsorbent for water treatment: batch and fixed-bed column adsorption of the nitrate anion. Applied Water Science. 2015:1-15.
10. Yoncheva K, Popova M, Szegedi A, Mihály J, Tzankov B, Lambov N, et al. Functionalized mesoporous silica nanoparticles for oral delivery of budesonide. Journal of Solid State Chemistry. 2014;211:154-61.
11. Yu M, Jambhrunkar S, Thorn P, Chen J, Gu W, Yu C. Hyaluronic acid modified mesoporous silica nanoparticles for targeted drug delivery to CD44-overexpressing cancer cells. Nanoscale. 2013;5(1):178-83.
12. Shah PV, Rajput SJ. A comparative in vitro release study of raloxifene encapsulated ordered MCM-41 and MCM-48 nanoparticles: A dissolution kinetics study in simulated and biorelevant media. Journal of Drug Delivery Science and Technology. 2017;41:31-44.
13. Rosen JE, Gu FX. Surface functionalization of silica nanoparticles with cysteine: a low-fouling zwitterionic surface. Langmuir. 2011;27(17):10507-13.
14. Ding Y, Shen SZ, Sun H, Sun K, Liu F, Qi Y, et al. Design and construction of polymerized-chitosan coated Fe 3 O 4 magnetic nanoparticles and its application for hydrophobic drug delivery. Materials Science and Engineering: C. 2015;48:487-98.
15. de Oliveira LFa, Bouchmella K, Gonçalves KdA, Bettini J, Kobarg Jr, Cardoso MB. Functionalized silica nanoparticles as an alternative platform for targeted drug-delivery of water insoluble drugs. Langmuir. 2016;32(13):3217-25.
16. Saroj S, Rajput SJ. Etoposide encapsulated functionalized mesoporous silica nanoparticles: Synthesis, characterization and effect of functionalization on dissolution kinetics in simulated and biorelevant media. Journal of Drug Delivery Science and Technology. 2017.
17. Deng L, Wang Y, Gong T, Sun X, Zhang Z-R. Dissolution and bioavailability enhancement of alpha-asarone by solid dispersions via oral administration. Drug development and industrial pharmacy. 2017;43(11):1817-26.

18. Marques M. Dissolution media simulating fasted and fed states. Dissolution Technologies. 2004;11(2):16-9.
19. Klein S. The use of biorelevant dissolution media to forecast the in vivo performance of a drug. The AAPS journal. 2010;12(3):397-406.
20. Salis A, Fanti M, Medda L, Nairi V, Cugia F, Piludu M, et al. Mesoporous silica nanoparticles functionalized with hyaluronic acid and chitosan biopolymers. Effect of functionalization on cell internalization. ACS Biomaterials Science & Engineering. 2016;2(5):741-51.
21. Huo J, Aguilera-Sigalat J, El-Hankari S, Bradshaw D. Magnetic MOF microreactors for recyclable size-selective biocatalysis. Chemical science. 2015;6(3):1938-43.
22. Senthilkumar R, Karaman DŞ, Paul P, Björk EM, Odén M, Eriksson JE, et al. Targeted delivery of a novel anticancer compound anisomelic acid using chitosan-coated porous silica nanorods for enhancing the apoptotic effect. Biomaterials science. 2015;3(1):103-11.
23. Zhao Y, Sun X, Zhang G, Trewyn BG, Slowing II, Lin VS-Y. Interaction of mesoporous silica nanoparticles with human red blood cell membranes: size and surface effects. ACS nano. 2011;5(2):1366-75.
24. Daryasari MP, Akhgar MR, Mamashli F, Bigdeli B, Khoobi M. Chitosan-folate coated mesoporous silica nanoparticles as a smart and pH-sensitive system for curcumin delivery. Rsc Advances. 2016;6(107):105578-88.
25. Akrami M, Khoobi M, Khalilvand-Sedagheh M, Haririan I, Bahador A, Faramarzi MA, et al. Evaluation of multilayer coated magnetic nanoparticles as biocompatible curcumin delivery platforms for breast cancer treatment. RSC Advances. 2015;5(107):88096-107.
26. Li J, Zheng L, Cai H, Sun W, Shen M, Zhang G, et al. Polyethyleneimine-mediated synthesis of folic acid-targeted iron oxide nanoparticles for in vivo tumor MR imaging. Biomaterials. 2013;34(33):8382-92.
27. Zhang Y, Zhi Z, Jiang T, Zhang J, Wang Z, Wang S. Spherical mesoporous silica nanoparticles for loading and release of the poorly water-soluble drug telmisartan. Journal of Controlled Release. 2010;145(3):257-63.
28. Kim JM, Chang SM, Kong SM, Kim K-S, Kim J, Kim W-S. Control of hydroxyl group content in silica particle synthesized by the sol-precipitation process. Ceramics International. 2009;35(3):1015-9.
29. de Oliveira Freitas LB, Bravo IJG, de Almeida Macedo WA, de Sousa EMB. Mesoporous silica materials functionalized with folic acid: preparation, characterization and release profile study with methotrexate. Journal of Sol-Gel Science and Technology. 2016;77(1):186-204.